EUROPEAN ORGANIZATION FOR NUCLEAR RESEARCH
CERN-EP/88-172
December 1st, 1988

CHARGED PARTICLE MULTIPLICITY DISTRIBUTIONS AT 200 AND 900 GeV C.M. ENERGY

UA5 Collaboration

Bonn[1], *Brussels*[2], *Cambridge*[3], *CERN*[4], *and Stockholm*[5]

R.E. Ansorge[3], B. Åsman[5], L. Burow[1], P. Carlson[5*], R.S. DeWolf[3], B. Eckart[1], G. Ekspong[5], I. Evangelou[4†], C. Fuglesang[4,5], J. Gaudaen[2§], C. Geich-Gimbel[1], B. Holl[1], K. Jon-And[5], F. Lotse[5], N. Manthos[4†], D.J. Munday[3], W. Pelzer[1], J.G. Rushbrooke[3], F. Triantis[4†], L. Van hamme[2], C. Walck[5], C.P. Ward[3], D.R. Ward[3], C.J.S. Webber[3], T.O. White[3], G. Wilquet[2], and N. Yamdagni[5]

Abstract

Multiplicity distributions of charged particles produced in non single-diffractive collisions between protons and antiprotons at centre of mass energies of 200 and 900 GeV are presented. The data were recorded in the UA5 streamer chambers at the CERN Collider, which was operated in a pulsed mode between the two energies. A new method to correct for acceptance limitations and inefficiencies based on the principle of maximum entropy has been used. Multiplicity distributions in full phase space and in intervals of pseudorapidity are presented in tabular form. The violation of KNO scaling in full phase space found by the UA5 group at an energy of 546 GeV is confirmed also at 200 and 900 GeV. The shape of the 900 GeV distribution in full phase space is narrower in the peak region than at 200 GeV but exhibits a pronounced high multiplicity tail. The negative binomial distribution fits data at 200 GeV in all pseudorapidity intervals and in small intervals at 900 GeV. In large intervals at 900 GeV, however, the negative binomial distribution fails to fit the data in the peak region of the distribution. Fits to the partially coherent laser distribution are also presented as well as comparisons with predictions of the Dual Parton, the Fritiof and the Pythia models.

[1] Physikalisches Institut der Universität Bonn, D-5300 Bonn, Federal Republic of Germany
[2] Inter-University Institute for High Energies (ULB-VUB), B-1050 Brussels, Belgium
[3] Cavendish Laboratory, Department of Physics, Cambridge University, Cambridge, CB3 OHE, UK
[4] CERN, CH-1211 Geneva 23, Switzerland
[5] Institute of Physics, University of Stockholm, S-113 46 Stockholm, Sweden
[*] Now at the Manne Siegbahn Institute, S-104 05 Stockholm, Sweden
[†] Also at the University of Ioannina, Ioannina, Greece.
[§] Also at the Universitaire Instellingen Antwerpen, Antwerp, Belgium.

(Submitted to Zeitschrift für PHysik C)

1 Introduction

Multiplicity scaling in the mean has been found to hold in the centre of mass energy range from 10 to 63 GeV for pp non single-diffractive events [1,2,3]. This finding was taken as support for the KNO scaling law [4]. The UA5 collaboration, however, showed that in $p\bar{p}$-collisions at 546 GeV [5] the scaling law was clearly broken. It was empirically found by the UA5 collaboration that multiplicity distributions of charged particles in non single-diffractive $p\bar{p}$-events can be successfully described by a negative binomial distribution with two fitted parameters [6]. It was also shown that it did not only fit multiplicity distributions in full phase space but also in central intervals of pseudorapidity [7]. The negative binomial distribution has been used to fit multiplicity distributions obtained with different beams at various energies with good results [8,9,10].

The possibility to extend the studies to still higher energies was opened by the development of a new pulsed mode of operation of the CERN SPS Collider [11]. The circulating beams of antiprotons and protons could be accelerated to a maximum beam energy of 450 GeV, held at this energy for several seconds and decelerated to 100 GeV in order to cool down the magnet system and then after a few seconds subjected to the same cycle again. The CERN SPS machine was tuned well enough such that beam losses in each cycle were negligible and the stray radiation background in the interaction region was no worse than during earlier runs at 546 GeV. The luminosity lifetime allowed several hours of data taking after each fill of the Collider. Details on the performance of the accelerator and other running conditions are given in ref. [12,13].

In this paper the results on multiplicity distributions obtained in proton-antiproton collisions at 200 and 900 GeV will be presented. It supersedes the earlier study [14], based on rather small samples, which now are included in the presented samples of several thousands of events.

2 Experimental procedure

2.1 The detector

The UA5 detector, shown in figure 1, was optimized for the study of charged particle multiplicity distributions for non single-diffractive events. The charged particles were detected in two large streamer chambers, one placed above, the other below the beam pipe. In order to minimize the production of electromagnetic showers by conversion of high energy photons the beam pipe was made of beryllium. The spatial resolution of tracks traversing the chambers was very good and since no magnetic field was applied, the tracks were straight and easy to measure. The geometrical acceptance of the chambers was about 95% in the pseudorapidity range $|\eta| < 3$, falling to zero at $|\eta| = 5$ (fig. 2a). Two systems of scintillator counter hodoscopes were used to trigger the high voltage pulse to the streamer chambers and the recording of the event on photographic film. For the present study the trigger logic required a coincidence between a beam crossing and at least one hit in each of the two trigger systems, which covered the pseudorapidity ranges $-5.6 < \eta < -2.0$ and $2.0 < \eta < 5.6$, respectively (fig. 2b). On triggered events the fraction of tracks seen was estimated by Monte Carlo simulation to be about 80% at 200 GeV and about 70% at 900 GeV. The different acceptances at the two energies are mainly due to different widths of the pseudorapidity distributions [15]. This minimum bias trigger excluded most of the single-diffractive events

and recorded about 95% of the non single-diffractive events. A detailed description of the detector has been published in ref. [16]. The results presented here are based on 4156 events at 200 GeV and 6839 events at 900 GeV.

2.2 Measurement and reconstruction of events

Both streamer chambers were equipped with three cameras, each with a pair of stereo views. The track images on film were measured on precision instruments and reconstructed in three dimensional space. Tracks with large residuals when fitted to a straight line were eliminated since such tracks often are due to slow secondary electrons. When all the tracks in an event had been reconstructed in space, the collision point of the interaction, the main vertex, and its associated tracks were determined using an iterative method. A preliminary vertex was placed on the beam axis at the position given by the average of the closest points along the beam axis. Tracks pointing too far from the vertex and tracks too close to each other were excluded. The latter cut was applied in order to eliminate electron-positron pairs created by photons in the beam pipe and to exclude decay products and hadrons created in secondary interactions. These cuts were different for different η-regions as optimized by Monte Carlo simulations. The vertex of each event was determined by minimizing the sum of squared distances from a point in space to the accepted primary tracks. With the new vertex the procedure started all over again and was repeated until the distance between two subsequent vertices was less then 0.25 cm. The final result was a sample of events characterized by a main vertex and its associated primary tracks. About 90% of all photon conversions and 97% of all hadronic secondary interactions are estimated to have been eliminated, whereas only 7% of the true primaries were excluded. The fraction of events with m observed primary tracks is denoted O_m. Corrections are necessary in order to compute the true distribution T_n of events with n charged particles. The method used to derive the set of T_n from the measured set of O_m is described in section 2.3.

2.3 A new method to determine the true multiplicity distribution

The number of observed vertex-associated tracks differs from the true number of charged particles due to the geometrical acceptance and to contamination by secondaries. In order to remove the contamination, cuts were applied to the data which unavoidably caused losses of some primary tracks. There is also a loss of events which fail to trigger the detector.

The trigger efficiency for each multiplicity ϵ_n and the probability P_{mn} that a true n-prong event would be observed as an event with m prongs were estimated using the UA5 Monte Carlo program which will be further discussed in the next section. In the limit of very large samples the observed multiplicity distribution is related to the corresponding true multiplicity distribution by the formula

$$O_m = \sum_{n=0}^{N} P_{mn}\epsilon_n T_n \quad (m = 0, 1...M) \tag{1}$$

where O_m is the fraction of events having m observed tracks, $\epsilon_n T_n$ is the fraction of triggered events having n primary charged particles produced, M and N are the maximum number of tracks and charged particles, respectively. The matrix elements P_{mn} and the trigger efficiencies were calculated for each pseudorapidity interval investigated. For fixed true multiplicity n, P_{mn} is a distribution in the observed number of m as illustrated in

figure 3. These distributions are narrow for small true multiplicities and broad for large true multiplicities. The mean values of the observed number of tracks are plotted versus the true number of particles for 900 GeV in full phase space in figure 4 as simulated by the UA5 Monte Carlo program. On the average there was a loss of particles, but as seen in figure 3 the observed multiplicity could in some events be somewhat larger than the true multiplicity.

It should be noted that eq. (1) is valid only for populations (the limit of infinitely many events) and that special care is necessary when using eq. (1) for finite samples. Solutions to eq. (1) are unphysical and often produce some negative T_n. In the experiment an unknown sample T_n was drawn from the likewise unknown population T'_n. It is obviously not possible to unfold the sampling processes to derive the sample T_n from the observed sample O_m, since further sampling processes were involved in the triggering and in the drawings from the P_{mn}-distributions. The aim must rather be to derive a population T'_n, which describes the data well in a statistical sense. This means that the differences $(O_m - \sum_{n=0}^{N} P_{mn}\epsilon_n T'_n)$ are expected to be of the order of the corresponding statistical errors σ_m and not equal to zero as would be the case if eq. (1) was solved. Thus we assume that T'_n should approximately satisfy the expectation value $E(\chi^2) = M$ and

$$\chi^2 = \sum_{m=0}^{M} \frac{(O_m - \sum_{n=0}^{N} P_{mn}\epsilon_n T'_n)^2}{\sigma_m^2} \tag{2}$$

The factor σ_m^2 is the quadratic sum of the statistical errors in O_m and in $P_{mn}\epsilon_n$ (due to the limited number of Monte Carlo events). Besides fulfilling eq.(2) with $\chi^2 \approx M$, T'_n should be such that the number of sign-changes is about $M/2$ in the sequence

$$O_m - \sum_n P_{mn}\epsilon_n T'_n, \qquad (m = 0, 1, 2, ...M) \tag{3}$$

An iterative method with smoothing between bins was applied earlier by the UA5 group to determine T'_n. It produced solutions which, however, suffered from defects in the form of oscillations superimposed on the smooth high multiplicity tail of the distribution. These oscillations are not physical but result from sampling fluctuations in data as was shown by applying the method to test samples [17]. We have therefore searched for an alternative and better method. Our new method to determine T'_n is based on maximizing the entropy for the distribution of triggered events, $t_n = \epsilon_n T'_n$, as defined by

$$S = -\sum_n t_n \ln t_n, \quad (0 \leq t_n \leq 1) \tag{4}$$

with linear constraints given by requiring that a set of observed moments based on eq. (1) are reproduced, i.e.

$$\sum_m m^q O_m = \sum_n \sum_m m^q P_{mn} t_n \tag{5}$$

for some values of q. Note that $q = 0$ gives the normalization condition. The maximum entropy method has been proven to be the only consistent way to choose one probability distribution out of many, all of which satisfy a set of linear constraints given by data [18].

In our case there is some arbitrariness in choosing the constraints. Our choice is motivated by the fact that for different q-values the function $m^q O_m$ emphasizes different regions of the variable m. High q-values emphasize the high multiplicity tail, $q = 1$ the region near

the mean multiplicity and negative q-values regions of m corresponding to low multiplicities. The chosen q-values belonged to the set $(q = -3, -2, -1, 0, 1, 2, 3, 4, 5, 6, 7)$ and were selected in such a way that the criteria based on eqs.(2) and (3) were fulfilled with the smallest possible subset of q's. The determination of t_n proceeded in steps. First, only two constraints were applied ($q = 0$ and $q = 1$). The t_n resulting from maximizing the entropy S was tested for its χ^2-value eq.(2), and the number of sign-changes, eq.(3). Constraints were added one by one as long as χ^2 decreased more than one unit. Empirically, it was found that after a certain number of steps the value of χ^2 became more or less constant, turning out to be about equal to M. The sign-change test was seldom critical. Furthermore the new method was proven to work well on test samples [19].

The number of constraints needed to satisfy the criteria varied from case to case. For some narrow distributions three constraints were sufficient, whereas the maximum number for any distribution was nine constraints. As an example, at 900 GeV in the interval $|\eta| < 0.2$ the subset $(q = 0, 1, 2, 3)$ was chosen whereas in full phase space the subset $(q = -3, -2....4, 5)$ was selected. The true multiplicity distribution, T'_n, was obtained from t_n through the relation $t_n = \epsilon_n T'_n$. By the normalization $P_n = T'_n / \sum T'_n$ the final corrected probability distribution was obtained. The P_n-distribution is not sensitive to which q-values were chosen as long as $\chi^2 \approx M$. Changes in individual bins of P_n are largest in the region of the peak, where the method may cause a systematic error of about the same magnitude as the statistical error.

If too many constraints were included, P_n in some cases developed wavy fluctuations superimposed on the otherwise smooth high multiplicity tail. We are convinced that such waves are artifacts produced by sampling fluctuations in the data. A criticism of our method could be that fine details of the true distribution may be lost. However, fine structures of P_n, should they exist, will be smeared by the $P_{mn}\epsilon_n$-factors and because of sampling fluctuations will most likely be lost in the observed O_m.

The iterative method used by UA5 in earlier publications is described in ref. [17]. The results from this method have been compared with the results given here and one example (the multiplicity distribution for full phase space at 900 GeV) is shown in figure 5. The first five moments of the distributions are the same. The distributions obtained by maximizing the entropy do not display the unphysical oscillations present when using the iterative method.

2.4 The Monte Carlo program

The Monte Carlo program used for corrections was developed by the UA5 collaboration. The event generator was not based on any specific model of multiparticle production, the philosophy was rather to create an empirical model within which our experimental results could be incorporated as they became available. The process of obtaining final results therefore became an iterative one.

The particles in the simulated events were tracked through the detector, allowing for interactions and scattering and the events were processed in the same way as the real measured events. The tracking program and the event generator are described in detail in ref. [20]. The discussion below will concentrate on those features of the event generator which are of importance for the correction of multiplicity distributions.

The first step in generating an event was to select the number of particles to be produced. A negative binomial distribution was chosen as it is known to fit the data approximately.

The probability matrix P_{mn}, as well as the trigger efficiency ϵ_n, are essentially independent of the input multiplicity distribution. What is essential for the determination of both P_{mn} and ϵ_n is to start from a correct pseudorapidity distribution. This point is discussed further in the next paragraph. The particles in the generated events were grouped into clusters in order to introduce short range correlations. The number of charged particles per cluster was made to follow an approximately Poissonian distribution with an average of about two. The clusters were assigned transverse momenta and were distributed in rapidity according to a uniform distribution with Gaussian tails. Leading particle effects were included by forcing one baryon and one antibaryon to have, with large probability, the largest and the smallest rapidity among the clusters. Energy and momentum was conserved in each event by transforming the cluster positions in p_y, p_z and rapidity (the x-axis is parallel to the beam direction) according to the method proposed in ref. [21]. Finally the clusters were made to decay isotropically.

It turns out that the estimated trigger efficiency for low multiplicities is quite sensitive to some assumptions of the empirical model. There are three features which are of importance. The pseudorapidity distribution at a given multiplicity must be right, since it determines the particle density in the pseudorapidity region $2 \leq |\eta| \leq 5.6$ covered by the trigger hodoscopes. Correlations are also important, since short range correlations increase the chance of all the particles missing one trigger plane and thus influence the value of the trigger efficiency. Both the pseudorapidity distribution and short range correlations have been measured by the UA5 collaboration. The pseudorapidity distributions at different multiplicities generated by the Monte Carlo program agree very well with data, see ref. [20], and the short range correlations have been incorporated in the event generator. Consequently, these two features do not contribute much to the systematic errors.

The main source of systematic error is the lack of knowledge of the distribution of longitudinal momenta of the leading baryons. Various assumptions for this distribution affect the trigger efficiency for events with low multiplicity. Since no measurement of leading baryons exists at the Collider, measurements at ISR have been used for guidance. In ref. [22] data in the centre of mass energy range from 14 to 28 GeV [23,24] are presented and it is concluded that the x_F-distribution for NSD events drops to zero between 0.95 and 1. In order to get an x_F-distribution similar to the one suggested in ref. [22], large values of x_F were suppressed according to a $(1-|x_F|)$-distribution (fig. 6). The dashed line in figure 6 shows the x_F-distribution of the leading baryon as it was generated by the Monte Carlo program with no suppression applied. This distribution was used in earlier publications [5,6,7,14]. In figure 7 is shown how the trigger efficiency depends on the x_F-distribution for the leading baryons. It is seen that the efficiency is independent of the x_F of the leading baryon at all values of x_F except for values close to one. This can be understood since it is unlikely to get any particles in the pseudorapidity range covered by the hodoscopes for events containing a baryon with large x_F.

In figure 8 an example is shown of the trigger efficiency estimated from the two versions of the UA5 Monte Carlo program having different x_F-distributions for the leading baryons. As seen in the figure, only the low multiplicities are affected by the different assumptions. The resulting systematic errors will be discussed in section 3.4.

3 Charged particle multiplicity distributions

The charged particle multiplicity distributions have been determined for full phase space and for a set of central acceptance intervals $|\eta| < \eta_c$ defined by the pseudorapidity cut η_c which was varied from 0.5 to 5.0 in steps of 0.5. Two smaller central intervals were added for which η_c is 0.2 and 0.25. We have also investigated intervals with the centre shifted from $\eta = 0$. This has been done for the full forward and full backward hemispheres and with the width of the interval chosen to be one unit of pseudorapidity and the centre positioned at $|\eta_0| = 0.5, 1,.. 3$. It should be noted that in the charged particle multiplicity distributions only particles from the primary vertex are included and not, for example, the decay products of K^0 and Λ.

3.1 Multiplicity distributions in full phase space

The normalized charged particle multiplicity distributions in full phase space at 200 and 900 GeV are given in table 1. The errors given contain both a statistical and a systematic component. The errors of the contents in neighbouring bins become necessarily strongly correlated. The statistical errors have been approximated by the square root of the corrected number of events in each bin. The systematic errors will be further discussed in section 3.4.

In figure 9 the distributions at 200 and 900 GeV are plotted in the z-variable ($z = n / <n>$). It is seen that the distribution at 900 GeV is broader than the one at 200 GeV, which confirms breaking of KNO scaling. A comparison with other energies are shown in figure 10 where the percentages of events having $z > 1.5$, $z > 2.0$ and $z > 2.5$ are plotted as a function of energy. The data points in the centre of mass energy range from 12 to 63 GeV are calculated from results in ref. [1,2,3] and the points at 546 GeV are given in ref. [16]. If KNO scaling would hold the percentages would be independent of energy. However, an increase in each percentage is seen at the Collider energies which shows that the distributions are getting relatively broader at these energies.

The significance of these changes in the shape can also be studied using moments of the distributions. The C-moments $C_q = < n^q > / < n >^q$ for $q = 2$ to 5 are plotted in figure 11 for the same experiments as in figure 10. Exact KNO scaling implies that all C_q-moments are energy independent. Although in the energy range from 30 GeV to 62 GeV all moments have almost constant values as was concluded in ref. [3], the UA5 values are significantly higher. The C-moments [1] of the distributions at 200 and 900 GeV are given in table 2 together with the mean values and the standard deviations. It has been emphasized by [25] that the physically most interesting moments are the reduced factorial moments ($F_q = < n(n-1)(n-2)...(n-q+1) > / < n >^q$) which also are given in table 2.

Apart from having a larger high multiplicity tail, the distribution at 900 GeV is different from the other distributions at multiplicities around the peak of the distribution. This is seen in figure 9 b where the distributions at 200 and 900 GeV are plotted on a linear scale. The distribution at 900 GeV is higher and more narrow in the neighbourhood of the peak

[1] The statistical errors of the C-moments for a given distribution are highly correlated. From the general formula for the covariance between two C-moments, valid for a sample of N_e events,

$$Cov(C_r, C_s) = \frac{1}{N_e}[C_{r+s} - rC_rC_{s+1} - sC_sC_{r+1} + C_rC_s\{rsC_2 - (r-1)(s-1)\}] \quad (6)$$

one finds that the correlation coefficients for adjacent C-moments are larger than 0.95 in all our cases.

and its position is shifted to a lower z-value (by definition the mean z=1). The shape at 900 GeV will be further discussed in section 4.2.

In view of recent interest in the entropy content of multiplicity distributions [26] we quote here $S = 3.03\pm0.03$ at 200 GeV and $S = 3.56\pm0.03$ at 900 GeV where the entropy is defined by

$$S = -\sum_n P_n \ln P_n \tag{7}$$

On the basis of the Simak-Sumbera-Zborovsky scaling rule $S/y_{max} = 0.417\pm0.003$ [26], where $y_{max} = ln((\sqrt{s} - 2m_p)/m_\pi)$, one would expect the values S =3.03±0.02 at 200 GeV and S =3.66±0.03 at 900 GeV.

3.2 Multiplicity distributions in symmetric pseudorapidity intervals

The multiplicity distributions in intervals defined by η_c = 5.0, 3.0, 1.5 and 0.5 at the c.m. energies of 200 and 900 GeV are given in table 3 and plotted in the z-variable in figure 12. The moments of the distributions are given in table 2. The distributions in small η-intervals are relatively broader than distributions in large intervals. This was also already observed at 546 GeV [7]. In figure 12 one sees that the narrow peak noticed in full phase space at 900 GeV also exists in the two largest intervals. In figure 13 the C_2-, C_3- and C_4-moments in various η-intervals are plotted versus the centre of mass energy. For comparison also NA22 data [27] and UA5 data at 546 GeV [7] are included in the figure. In large pseudorapidity intervals, like in full phase space, the C-moments increase with energy, whereas they decrease in small intervals. They are approximately independent of energy between the centre of mass energies of 22 GeV and 900 GeV in the central region defined by $\eta_c = 0.5$.

The scaled entropy, S/y_{max} as a function of the scaled pseudorapidity η_c/y_{max} is plotted in figure 14 for our new data at 200 and 900 GeV. In contrast to full phase space, where only even multiplicities are allowed due to charge conservation, both even and odd multiplicities occur in pseudorapidity intervals. For all multiplicities the entropy, S(all n), differs from the one computed for only even multiplicities, S(even n). One can show that S(all n)=S(even n) + $ln2$ holds whenever the even and odd multiplicities comprise each 1/2 of the total, which is approximately true in our case. Close to full phase space the odd multiplicities gradually disappear and S(all n) =S(even n). In figure 14 S(all n)/y_{max} is plotted and in order to compare with results on entropy scaling [26], also S(even n) /y_{max}, where n=0 has been excluded. At 200 GeV the data are in agreement with the curve but at 900 GeV the points are systematically above the curve in small pseudorapidity intervals.

3.3 Multiplicity distributions for non-symmetric pseudorapidity intervals

In table 4 the moments obtained in η-intervals one unit wide with displaced centres positioned at $|\eta_0| = 0.5, 1, ...3$ are given. The C-moments decrease when the centre of the interval is moved further from η= 0 at all energies, as long as only the pseudorapidity plateau is investigated. This means that the relative fluctuations are largest in the central region. Outside the pseudorapidity plateau the C-moments show no clear trend. The moments of the multiplicity distributions in the forward and backward hemispheres are also given in table 4.

3.4 Systematic errors

The systematic errors are largest for the lowest multiplicities and they dominate the errors shown in table 2. The main source of systematic errors for the low multiplicities is the uncertainty in the trigger efficiency. The magnitude of the errors has been estimated by varying the $|x_F|$-distribution of the leading baryon in the Monte Carlo event generator as discussed in section 2.4. The choice of method to determine the true multiplicity distribution also causes uncertainties for the low multiplicities. We have estimated the errors by comparing the output from the maximum entropy method used in this paper with the iterative method used earlier. Furthermore according to Monte Carlo simulations [12] we have an uncertainty of about 2% due to single-diffractive events in the non single-diffractive sample which is not corrected for. This contamination also affects the low multiplicities.

As discussed in section 2.3 the derived T'_n-distribution depends slightly on the constraints applied in the maximum entropy method. The resulting errors are largest in the region of the peak but they are generally smaller or of the same size as the statistical ones. For the large multiplicities the uncertainty comes mainly from the cuts made in the vertex finding program. Different cuts have been made to estimate these errors.

4 Parametrisations and models

In this section some parametrisations of the multiplicity distributions are discussed. Data are also compared to three models, the Dual Parton, Fritiof and Pythia models which all exist in Monte Carlo versions.

The fits were all performed to the observed and not to the corrected distributions in order to avoid the complication introduced by the strongly correlated errors between bin contents in the latter distribution. When a certain functional form $F_n(x_1, x_2, ...)$ was assumed for the true multiplicity distribution, its free parameters x_1,x_2,... were fitted to the observed data with the least squares method. The assumed true form was inserted in:

$$\chi^2 = \sum_m \frac{(O_m - \sum_{n=1}^{N} P_{mn}\epsilon_n F_n(x_1, x_2, ...))^2}{\sigma_m^2} \tag{8}$$

which was minimized in the allowed parameter space (cf. eqs. (1) and (2)) and the minimum of $\chi^2(=\chi_0^2)$ computed from eq. (8). A fit is classified in this paper as acceptable if the probability for a χ^2 larger than χ_0^2 exceeds 0.1%. Bins for which the systematic error was estimated to be larger than the statistical error were excluded from the fits. The number of excluded bins varied from zero to four.

4.1 Fits to the negative binomial distribution

The negative binomial distribution (NBD) is defined by

$$P_n(\overline{n}, k) = \left(\begin{array}{c} n+k-1 \\ k-1 \end{array} \right) \left(\frac{\frac{\overline{n}}{k}}{1+\frac{\overline{n}}{k}} \right)^n \frac{1}{(1+\frac{\overline{n}}{k})^k} \tag{9}$$

The parameter $\overline{n}$ gives the average of the distribution and at a fixed $\overline{n}$ the parameter k determines the shape of the distribution. The NBD turns into a Poisson distribution when $k^{-1} \to 0$ and a geometrical distribution when $k = 1$. In the limit $\overline{n} \to \infty$ it tends

to a gamma distribution. If k is a negative integer eq. (9) gives the ordinary binomial distribution. Moments of the NBD can be expressed in the parameters, e.g.

$$C_2 = 1 + \frac{1}{k} + \frac{1}{\overline{n}} \tag{10}$$

$$C_3 = 1 + \frac{3}{k} + \frac{2}{k^2} + \frac{3}{\overline{n}}\left(1 + \frac{1}{k}\right) + \frac{1}{\overline{n}^2} \tag{11}$$

$$C_4 = 1 + \frac{6}{k} + \frac{11}{k^2} + \frac{6}{k^3} + \frac{6}{\overline{n}}\left(1 + \frac{3}{k} + \frac{2}{k^2}\right) + \frac{7}{\overline{n}^2}\left(1 + \frac{1}{k}\right) + \frac{1}{\overline{n}^3} \tag{12}$$

$$D_2 = \overline{n} + \frac{\overline{n}^2}{k} \tag{13}$$

Fits of the NBD to full phase space data are shown in figure 15 and 16. Only even values of n are used in eq. (9) because of charge conservation, and the distribution is renormalized. In figure 15 the corrected multiplicity distribution is shown and in figure 16 the observed distribution together with the corresponding values for the fitted negative binomial distribution[2]. The resulting values of the parameters and χ_0^2/NDF (where NDF is the number of degrees of freedom) are given in table 5. The published fit at 546 GeV was remarkably good [6] and this is now also the case at 200 GeV. At 900 GeV, however, the fit is unacceptable. A study of the contributions to χ_0^2 bin by bin shows that the main contributions come from the bins $12 < m < 15$ where the data points are systematically above the NBD-points and from the bins $26 < m < 36$ where the data points are systematically below. This deviation between data and the fitted negative binomial distribution is also clearly seen in figure 16. The corresponding true multiplicities are in the regions around 20 and 45. The high multiplicity tail, however, is very well represented by the fitted NBD. The moments of the fitted NBD are almost the same as the moments of the corrected distribution. Inserting the fitted values $\overline{n}$=35.2 and k=3.7 in eqs. (10) to (12) we find C_2=1.30 (1.30±0.01), C_3=2.07 (2.08±0.03), C_4=3.9 (3.9±0.1) and also C_5=8.4 (8.9±0.5), with the moments of the data given in parentheses. It seems that in this sense the overall features of the data can be fairly well described by the NBD, but there is some localized structure near the peak which is not accounted for by the NBD.

When phase space is limited with symmetric cuts in pseudorapidity ($|\eta| < \eta_c$), the fits (now with n both odd and even) to the 900 GeV data get less bad with decreasing η_c, and for $\eta_c \leq 2.5$ the fits are acceptable. The structures giving the large χ^2 contributions for full phase space move to lower multiplicities when η_c is decreased. Results of the fits to the data in the pseudorapidity intervals defined in section 3.2 are presented in table 5. The χ_0^2/NDF-values at 200 GeV show that all fits are good. In figure 17 the k parameter is plotted as a function of the cut parameter η_c at the c.m. energies 200 and 900 GeV as well as 546 GeV [7]. Values from unacceptable fits are not shown. The k value increases roughly linearly with η_c, with a slope and intercept that both decrease with energy.

Fits have also been made to multiplicity distributions in non-central pseudorapidity intervals, with a width $\Delta\eta$=1 and the centres positioned at $|\eta_0|$ =0.5, 1,..., 3. The resulting values of k and χ_0^2/NDF are given in table 6. All fits are satisfactory. The k parameter increases when the centre is moved outwards.

[2]i.e. the values of the second term in the numerator of eq. (8), with F_n given by eq. (9).

4.2 The shape of the multiplicity distribution at 900 GeV

As discussed in sections 3.1 and 4.1 the shape of the 900 GeV distribution differs from those at lower energies. This could be due to errors or to a physical process. We have made detailed investigations of possible systematic errors and we give an account here. A comparison between multiplicity distributions measured in our different laboratories with different equipment shows that all the measuring machines give consistently the same result. A division of the total sample of events into subsamples containing events recorded close in time was made in order to study if the shape of the distribution depended on the running conditions. No systematic change was observed. No asymmetry between the multiplicity distribution in the upper and the lower chamber or between the forward and backward hemisphere has been found. There is also no contamination of events at the energy of 200 GeV in the event sample at 900 GeV. The events were recorded on the same film and were automatically energy labeled. If the labeling had malfunctioned during the run a contamination of events at 200 GeV, having lower multiplicity, could have been mistaken as 900 GeV events. However, an independent test exists, since the vertical position of the beam was different at the two different energies (probably due to magnet saturation at 900 GeV). No contamination was found as seen from the measured vertical coordinates of the events labeled "900 GeV". In conclusion no systematic error has been found which could influence the shape of the 900 GeV multiplicity distribution.

The events with a multiplicity of about 12-15 tracks were carefully investigated to see if the excess could have been caused by single-diffractive events produced with a much higher rate than expected from extrapolations from lower energies [12]. The pseudorapidity distribution, however, had a shape similar to the one generated in Monte Carlo simulations for ordinary events. Furthermore, the investigation of forward-backward multiplicity correlations showed no sign of an excess of single-diffractive events. A study of correlations between the central region in pseudorapidity and the forward and backward regions shows that it was not likely that the excess was caused by a large production of double diffractive events.

4.3 Fits to the partially coherent laser distribution

A more general formula than the negative binomial distribution, called the partially coherent laser distribution (PCLD) (or the generalized Glauber-Lachs or Laguerre distribution), which interpolates between the negative binomial and the Poisson distributions has been suggested [28,29,30] to be the appropriate distribution for multiplicities, motivated by quantum statistical arguments. In this picture, particles are emitted from k independent and identical cells, which have a chaotic and a coherent part. The probability to produce n particles is then

$$P_n(\mathcal{N},\mathcal{S},k) = \frac{(\mathcal{N}/k)^n}{(1+\mathcal{N}/k)^{n+k}} exp(-\frac{\mathcal{S}}{1+\mathcal{N}/k}) L_n^{k-1}(-\frac{k\mathcal{S}/\mathcal{N}}{1+\mathcal{N}/k}) \qquad (14)$$

where $\mathcal{N}$ and $\mathcal{S}$ are the average number of particles from the chaotic and coherent parts, respectively (i.e. $\overline{n} = \mathcal{N} + \mathcal{S}$), and L_n^r denotes the n:th Laguerre polynomial of order r. When the chaoticity is 100% the PCLD becomes a negative binomial distribution and when the chaoticity is zero it becomes a Poisson distribution. Although k is an integer in the original derivation of eq. (14) [28,29] one can assume that it can be generalized to any real number $k > 0$.

The PCLD was fitted to charge particle multiplicity distributions in full phase space at 200 and 900 GeV. The fitting was done with k fixed to 1, 2 and 3, and also with k as a free parameter. In all cases the fits were acceptable at 200 GeV, whereas at 900 GeV the fits were never good. When k was a free parameter, the chaoticity was consistent with being 100% at both energies, i.e. the data preferred the NBD limit.

A comparison of PCLD with multiplicity distributions in several symmetric η-intervals as well as full phase space at 546 GeV has been presented in ref. [31]. Again eq. (14) was fitted with k fixed at 1, 2 and 3, respectively, and none of the k values results in a good fit in all intervals of pseudorapidity, although $k = 1$ gives a bad fit only for $\eta_c = 3$. On the other hand in some intervals several k values give acceptable fits and one cannot discriminate between them. With the parameter k free, the fits result in k values which are in general the same or slightly less than for the NBD fits. The PCLD fits are only marginally better than the NBD fits.

We conclude that those of our multiplicity distributions which can be described with the NBD can also be described with the PCLD but only if the k parameter is allowed to vary with the size of the studied pseudorapitity interval. This fact is trivial, since the NBD is a special case of the PCLD. A more interesting conclusion is that the 900 GeV distributions which cannot be well described with the NBD, cannot be well described with the PCLD either.

4.4 Comparison of the results with model predictions

The Dual Parton (DPM), Pythia and Fritiof models, based on the assumption that hadrons are produced via chains or strings, are compared to the UA5 multiplicity distributions. In all models the validity of jet universality has been assumed for the fragmentation of the chains (strings). In particular for the Pythia and the Fritiof model the e^+e^- hadronization process, which may be simulated by the Lund Monte Carlo program [32], is used. In the DPM either the e^+e^- hadronization process or the parton fragmentation process, which has been studied in deep inelastic lepton hadron reactions, is used for the chain fragmentation.

In the DPM [33,34,35] chains are assumed to be formed by Pomeron exchanges, where each Pomeron gives rise to two chains stretched between either valence or sea partons. At low energies the dominating process is the single Pomeron exchange, which leads to two chains stretched between the valence partons. With increasing energy additional Pomeron exchanges, which form chains stretched between sea partons, occur. Since the sea partons carry only a small fraction of momentum of the incident hadrons these chains are concentrated in the central rapidity region. Thus these extra chains might explain the observed KNO scaling violation and the increase of the central particle density with increasing energy. The distribution of the number of Pomerons is obtained from perturbative Reggeon calculus and from data on the total, elastic and diffractive cross sections. For the comparison here, a DPM Monte Carlo version [35] tuned to 546 GeV multiplicity data [36] has been used.

In the Fritiof model [37] it is assumed that a hadron behaves as a vortex line (the confining colour field) in a superconducting medium (the vacuum). The vortex line has a thin hard core containing most of the energy, and an exponentially damped field around the core. When two hadrons pass each other the extended fields overlap and a lot of independent elastic scatterings between line-pieces are produced. The four-momentum transferred in all the scatterings are summed up and put at the end of the string. The main

part of the momentum transfer is longitudinal, thus a hadron-hadron collision will result in two strings which in general are linearly stretched out in the beam direction with a diquark in the leading end and a quark in the retarding end. In addition, Fritiof includes gluon bremsstrahlung and possibly one hard scattering, which both gives kinks (excitations) to the two strings.

In Pythia [38,39] hard or semihard scattering between partons results in strings. In the first scattering two strings are stretched between quarks and further scatterings give rise to additional strings or kinks on strings. The number of scatterings is determined by an impact parameter, and the hadronic matter distribution is assumed to be double Gaussian. Wherever possible, perturbative QCD is used. A smooth damping at low p_T is used instead of a cutoff. The model has a double diffractive component, with a dM^2/M^2 spectrum for the diffractive systems, and each system is represented by a string from a diquark in the forward end to a quark in the other end.

The comparison of the model distributions and the UA5 data was made for the observed multiplicity distributions (like the NBD fits) for full phase space and also for the limited rapidity intervals. The multiplicity distributions of the models were multiplied by the trigger efficiency and passed through the acceptance matrix P_{mn} in order to give the predicted observed model distributions. In figure 18 the three models are compared to UA5 data in four different symmetric rapidity intervals, η_c= 0.5, 1.5, 3.0 and 5.0 and for the two energies. All the models in their present form are in broad agreement with the data though there clearly are differences in details. However, the χ_0^2 is generally much too large with the exceptions that in some small pseudorapidity intervals the DPM and Pythia models describe the data satisfactorily.

The analytical model [34] based on the Dual Parton model exhibits a peak at low multiplicity at 900 GeV, a medium multiplicity shoulder and a sizeable high multiplicity tail, qualitatively similar to our 900 GeV data.

5 Conclusions

The average charged particle multiplicities for non single-diffractive events are 21.4±0.2±0.4 at 200 GeV c.m. energy and 35.6±0.2±0.9 at 900 GeV with standard deviations of 10.8±0.1±0.3 and 19.5±0.2±0.3 , respectively. The ratio between the standard deviation and the mean is increasing with energy which shows that the distributions are getting relatively broader with increasing energy. The KNO scaling violation which was observed by the UA5 collaboration at 546 GeV c.m. energy is also observed at 200 and 900 GeV. At 900 GeV the peak of the distribution is relatively more narrow than at lower energies. The narrow peak seen in full phase space at 900 GeV is also seen in large pseudorapidity intervals but disappears in small intervals. A description in terms of the negative binomial distribution with two fitted parameters, which worked well at the c.m. energy of 546 GeV and at energies below 60 GeV, is again successfully applied to the 200 GeV data. However, at 900 GeV the negative binomial distribution fails to describe the multiplicity distributions in central pseudorapidity intervals larger than five units wide. The conclusion must be that the negative binomial distribution is not sufficient to describe the full phase space multiplicity distribution at 900 GeV c.m. energy. The origin of this failure has been traced to a pronounced narrow peak which is a new feature of the 900 GeV multiplicity distribution. In small intervals, however, the negative binomial distribution fits the data very well. The

partially coherent laser distribution has been fitted to data at 200 and 900 GeV. It has been found that when the negative binomial fails to fit data so does the partially coherent laser distribution. The Dual Parton, Pythia and Fritiof models are in broad agreement with data but there are clear differences in details.

Acknowledgements. We acknowledge with thanks the financial support of the Brussels group by the National Foundation for Fundamental Research and the Inter-University Institute for Nuclear Sciences, of the Bonn group by the Bundesministerium für Wissenschaft und Forschung, of the Cambridge group by the UK Science and Engineering Research Council, and of the Stockholm group by the Swedish Natural Science Research Council. Last but not least, we acknowledge the contribution of the engineers, scanning and measuring staff of all our laboratories.

References

[1] H.B. Bialkowska et al., Nucl. Phys. **B110** (1976) 300 ;
V.V. Ammosov et al., Phys. Lett. **42B** (1972) 519.

[2] J. Whitmore et al., Phys. Rep. **10C** (1974) 273 ;
C. Bromberg et al., Phys. Rev. Lett. **31** (1973) 1563 ;
A. Firestone et al., Phys. Rev. **D10** (1974) 2080 ;
S. Barish et al., Phys. Rev. **D9** (1974) 2689 ;
W.M. Morse et al., Phys. Rev. **D15** (1977) 66 .

[3] A. Breakstone et al., Phys. Rev. **D30** (1984) 528 .

[4] Z. Koba, H.B. Nielsen and P. Olesen, Nucl. Phys. **B40** (1972) 317 .

[5] UA5 Collaboration, G.J. Alner et al., Phys. Lett. **138B** (1984) 304 .

[6] UA5 Collaboration, G.J. Alner et al., Phys. Lett. **160B** (1985) 199 .

[7] UA5 Collaboration, G.J. Alner et al., Phys. Lett. **160B** (1985) 193 .

[8] M. Adamus et al., Phys. Lett. **177B** (1986) 239 ;
M. Adamus et al., Z. Phys. **C32** (1986) 475 M. Adamus et al., Z. Phys. **C37** (1988) 215.

[9] M. Derrick et al., Phys. Lett. **168B** (1986) 229 ;
M. Derrick et al., Phys. Rev. **D34** (1986) 3304 ;
F. Dengler et al., Z. Phys. **C33** (1986) 187.

[10] M. Arnedo et al., Z. Phys. **C35** (1987) 335 ;
R. Ammer et al., Phys. Lett. **178** (1986) 124 ;
J.L. Bailly et al., Z. Phys. **C40** (1988) 215.

[11] J.G. Rushbrooke, CERN/EP 82-6 (1982).

[12] UA5 Collaboration, G.J. Alner et al., Z. Phys **C32** (1986) 153.

[13] R. Laukner, IEEE Trans. Nucl. Sci. **NS-32** (1985) 1653.

[14] UA5 Collaboration, G.J. Alner et al., Phys. Lett. **167B** (1986) 476 .

[15] UA5 Collaboration, C.J. Alner et al., Z. Phys. **C33** (1986) 1 .

[16] UA5 Collaboration, G.J. Alner et al., Phys. Rep. **154** (1987) 247 .

[17] B. Åsman, "From tracks on film to corrected multiplicity distributions" University of Stockholm, USIP Report **17** (1985).

[18] E.T. Jaynes, Phys. Rev. **106** (1957) 620;
J.E. Shore and R.W. Johnson, IEEE Trans. Inform. Theory **IT-26** (1980) 26 and **IT-29** (1983) 942 ;
Y. Tikoschinsky, N.K. Tishby and R.D. Levine, Phys. Rev. Lett. **52** (1984) 1357 ;
J. Skilling, Nature **309** (1984) 748 .

[19] C. Fuglesang, A method for correcting observed distributions of for example, multiplicities using the maximum entropy principle, CERN prepront, in preparation.

[20] UA5 Collaboration, G.J. Alner et al., Nucl. Phys. **B291** (1987) 445 .

[21] S. Jadach, Comp. Phys. Comm. **9** (1975) 297 .

[22] M. Basile et al., Lett. Nuovo Cim. **38** (1983) 359 .

[23] J.W. Chapman et al., Phys. Rev. Lett. **32** (1974) 257 .

[24] P. Capilappi et al., Nucl. Phys. **B70** (1974) 1.

[25] A. Bialas and R. Peschanski, Nucl.Phys. **B273** (1986) 703.

[26] V. Simak, M. Sumbera and I. Zborovsky, Proc. Int. Europhysics Conference on High-Energy Physics, Uppsala 1987, page 476 .

[27] M. Adamus et al., Z. Phys. **C37** (1988) 215.

[28] P. Carruthers and C.C. Shih, Phys. Lett. **137B** (1984) 425 ;
P. Carruthers and C. Shih, Int. J. Mod. Phys. **A2** (1987) 1447 .

[29] M. Biyajima, Prog. Theor. Phys. **69** (1983) 966 .

[30] M. Weiner, Proc. Hadronic Matter in Collision, Proc. LESIP II Workshop, Santa Fe 1986, page 106.

[31] C. Fuglesang, Thesis, University of Stockholm. 1987.

[32] B. Andersson et al., Phys. Rep. **97** (1983) 31 .

[33] A. Capella et al., Phys. Lett. **B81** (1979) and Z. Phys. **C3** (1980) 329;
A. Capella and J. Tran Than Van, Z. Phys. **C23** (1984) 165;
A. Capella, A. Staar and J. Tran Thanh Van, Phys. Rev. D32 (1985) 2; .

[34] A.B. Kaidalov and K.A. Ter-Martirosyan, Phys. Lett. **B117** (1982) 247;
K.A. Ter-Martirosyan, ITEP 86-121, Moscow, Atom Inform., 1986.

[35] P. Aurenche et al., Z. Phys. **C23** (1984) 67,**C26** (1984) 279
and Phys. Lett. B147 (1984) 212;
P. Aurenche et al., Phys. Rev. **33D** (1986) 1876 .

[36] B. Holl, Diplomarbeit, University of Bonn. BONN-IR-15, 1986.

[37] B. Andersson et al., Nucl. Phys. **B281** (1987) 284 ;
B. Andersson et al., LU TP 87-6(1987).

[38] T Sjöstrand and M. van Zijl, Phys. Rev. **36D** (1987) 2019.

[39] H.U. Bengtsson and T. Sjöstrand, Comp. Phys. Comm. **46** (1987) 43 ;
M. Bengtsson and T Sjöstrand, Comp. Phys. Comm. **43** (1987) 367 .

Table 1: The corrected charged particle multiplicity distributions in full phase space at the c.m. energy of 200 and 900 GeV given as probabilities. The errors contain both a statistical and a systematic component and are highly correlated between bins. When the number of events per bin falls below 5, the bins are grouped and the entry represents the corresponding sum of the included bins.

200 GeV		900 GeV	
n	P_n	n	P_n
2	0.008±0.004	2-6	0.007±0.009
4	0.014±0.007	8	0.014±0.002
6	0.025±0.009	10	0.018±0.002
8	0.044±0.005	12	0.025±0.003
10	0.062±0.005	14	0.033±0.003
12	0.075±0.005	16	0.041±0.003
14	0.084±0.006	18	0.050±0.004
16	0.087±0.006	20	0.053±0.004
18	0.083±0.006	22	0.057±0.004
20	0.077±0.006	24	0.056±0.004
22	0.069±0.006	26	0.054±0.004
24	0.060±0.005	28	0.050±0.004
26	0.053±0.005	30	0.047±0.004
28	0.044±0.004	32	0.042±0.003
30	0.038±0.004	34	0.039±0.003
32	0.032±0.004	36	0.036±0.003
34	0.027±0.003	38	0.033±0.003
36	0.023±0.003	40	0.030±0.003
38	0.019±0.003	42	0.028±0.003
40	0.016±0.003	44	0.025±0.003
42	0.013±0.002	46	0.023±0.003
44	0.011±0.002	48	0.021±0.002
46	0.009±0.002	50	0.020±0.002
48	0.007±0.002	52	0.019±0.002
50	0.005±0.002	54	0.017±0.002
52	0.004±0.001	56	0.016±0.002
54	0.003±0.001	58	0.015±0.002
56	0.002±0.001	60	0.014±0.002
58	0.0014±0.0009	62	0.013±0.002
60-62	0.0016±0.0009	64	0.012±0.002
64-76	0.0013±0.0007	66	0.011±0.002
		68	0.010±0.002
		70	0.009±0.002
		72	0.008±0.002
		74	0.007±0.001
		76	0.007±0.001
		78	0.006±0.001
		80	0.005±0.001
		82	0.004±0.001
		84	0.004±0.001
		86	0.003±0.001
		88	0.0029±0.0009
		90	0.0025±0.0008
		92	0.0022±0.0008
		94	0.0018±0.0007
		96	0.0015±0.0007
		98	0.0013±0.0006
		100	0.0011±0.0006
		102	0.0009±0.0006
		104	0.0008±0.0005
		106-108	0.0012±0.0006
		110-112	0.0008±0.0005
		114-120	0.0009±0.0005
		122-136	0.0008±0.0005

Table 2: Moments of the multiplicity distributions at 200 and 900 GeV in central intervals $|\eta| < \eta_c$ and in full phase space (denoted with $*$). The average charged particle multiplicity $< n >$, the standard deviation $D_2 = < (n - < n >)^2 >^{1/2}$, the first four C_q-moments, and the reduced factorial moments, are given. The C-moments are defined by $C_q = < n^q > / < n >^q$ and the reduced factorial moments by $F_q = < n(n-1)(n-2)...(n-q+1) > / < n >^q$). The first error is statistical, the second systematic.

200 GeV			
η_c	$< n >$	D_2	$< n > / D_2$
0.2	0.97±0.02 ± 0.04	1.20±0.02 ± 0.05	0.81±0.01 ± 0.03
0.25	1.22±0.02 ± 0.04	1.40±0.02 ± 0.05	0.87±0.01 ± 0.03
0.5	2.50±0.04 ± 0.08	2.37±0.03 ± 0.08	1.06±0.01 ± 0.03
1.0	5.17±0.06 ± 0.12	4.23±0.05 ± 0.12	1.22±0.01 ± 0.03
1.5	7.94±0.09 ± 0.21	5.93±0.08 ± 0.19	1.34±0.01 ± 0.03
2.0	10.7±0.1 ± 0.3	7.5±0.1 ± 0.2	1.43±0.01 ± 0.04
2.5	13.2±0.1 ± 0.3	8.8±0.1 ± 0.3	1.51±0.01 ± 0.05
3.0	15.5±0.1 ± 0.4	9.7±0.1 ± 0.3	1.59±0.02 ± 0.07
3.5	17.4±0.2 ± 0.4	10.4±0.1 ± 0.3	1.68±0.02 ± 0.07
4.0	18.9±0.2 ± 0.4	10.8±0.1 ± 0.3	1.75±0.02 ± 0.07
4.5	19.9±0.2 ± 0.4	11.0±0.1 ± 0.3	1.81±0.02 ± 0.07
5.0	20.5±0.2 ± 0.4	11.0±0.1 ± 0.3	1.86±0.02 ± 0.07
*	21.4±0.2 ± 0.4	10.8±0.1 ± 0.3	1.98±0.02 ± 0.08
900 GeV			
η_c	$< n >$	D_2	$< n > / D_2$
0.2	1.43±0.02 ± 0.05	1.69±0.02 ± 0.04	0.85±0.01 ± 0.02
0.25	1.80±0.02 ± 0.05	2.01±0.02 ± 0.04	0.89±0.01 ± 0.02
0.5	3.61±0.04 ± 0.12	3.50±0.04 ± 0.10	1.03±0.01 ± 0.02
1.0	7.38±0.08 ± 0.27	6.41±0.08 ± 0.13	1.15±0.01 ± 0.03
1.5	11.2±0.1 ± 0.3	9.0±0.1 ± 0.2	1.24±0.01 ± 0.03
2.0	15.1±0.1 ± 0.5	11.5±0.1 ± 0.2	1.31±0.01 ± 0.03
2.5	18.8±0.2 ± 0.7	13.8±0.2 ± 0.2	1.37±0.01 ± 0.03
3.0	22.4±0.2 ± 0.7	15.7±0.2 ± 0.3	1.42±0.01 ± 0.03
3.5	25.6±0.2 ± 0.8	17.3±0.2 ± 0.3	1.48±0.01 ± 0.04
4.0	28.3±0.2 ± 0.9	18.4±0.2 ± 0.3	1.54±0.01 ± 0.05
4.5	30.6±0.2 ± 0.9	19.2±0.2 ± 0.3	1.60±0.01 ± 0.06
5.0	32.5±0.2 ± 0.9	19.6±0.2 ± 0.3	1.66±0.01 ± 0.07
*	35.6±0.2 ± 0.9	19.5±0.2 ± 0.3	1.82±0.01 ± 0.10

continuation of table 2

200 GeV				
η_c	C_2	C_3	C_4	C_5
0.2	2.54±0.05 ± 0.07	8.5±0.4 ± 0.5	36±4 ± 4	180±40 ± 30
0.25	2.32±0.04 ± 0.05	7.1±0.3 ± 0.4	27±3 ± 3	120±30 ± 20
0.5	1.90±0.02 ± 0.04	4.8±0.2 ± 0.3	15±1 ± 1	52±8 ± 5
1.0	1.67±0.01 ± 0.03	3.7±0.1 ± 0.1	9.7±0.7 ± 0.9	29±4 ± 3
1.5	1.56±0.01 ± 0.03	3.16±0.08 ± 0.11	7.7±0.4 ± 0.5	22±4 ± 3
2.0	1.49±0.01 ± 0.03	2.86±0.07 ± 0.09	6.6±0.4 ± 0.5	18±2 ± 1
2.5	1.44±0.01 ± 0.03	2.65±0.06 ± 0.09	5.8±0.3 ± 0.4	15±2 ± 1
3.0	1.40±0.01 ± 0.03	2.46±0.05 ± 0.08	5.1±0.2 ± 0.3	12±1 ± 1
3.5	1.35±0.01 ± 0.03	2.27±0.04 ± 0.08	4.5±0.2 ± 0.3	10.0±0.8 ± 0.8
4.0	1.32±0.01 ± 0.03	2.15±0.04 ± 0.08	4.1±0.2 ± 0.3	8.9±0.7 ± 0.7
4.5	1.30±0.01 ± 0.03	2.07±0.04 ± 0.08	3.8±0.1 ± 0.3	7.9±0.6 ± 0.7
5.0	1.29±0.01 ± 0.03	2.00±0.03 ± 0.08	3.6±0.1 ± 0.3	7.2±0.5 ± 0.7
*	1.26±0.01 ± 0.03	1.88±0.03 ± 0.08	3.2±0.1 ± 0.3	6.2±0.4 ± 0.5
900 GeV				
η_c	C_2	C_3	C_4	C_5
0.2	2.40±0.03 ± 0.04	8.3±0.4 ± 0.5	39±4 ± 4	240±50 ± 50
0.25	2.25±0.03 ± 0.04	7.3±0.3 ± 0.4	31±2 ± 2	170±20 ± 10
0.5	1.94±0.02 ± 0.04	5.4±0.2 ± 0.3	19±1 ± 1	80±10 ± 10
1.0	1.75±0.02 ± 0.04	4.4±0.1 ± 0.1	14.1±0.9 ± 1.2	56±7 ± 5
1.5	1.65±0.01 ± 0.03	3.7±0.1 ± 0.1	10.5±0.7 ± 0.9	35±5 ± 3
2.0	1.59±0.01 ± 0.03	3.37±0.08 ± 0.12	8.8±0.5 ± 0.7	27±3 ± 2
2.5	1.53±0.01 ± 0.03	3.11±0.07 ± 0.12	7.7±0.4 ± 0.5	22±2 ± 1
3.0	1.50±0.01 ± 0.03	2.93±0.06 ± 0.10	7.0±0.3 ± 0.5	19±2 ± 1
3.5	1.45±0.01 ± 0.03	2.74±0.05 ± 0.10	6.2±0.3 ± 0.5	16±1 ± 1
4.0	1.42±0.01 ± 0.03	2.58±0.05 ± 0.10	5.6±0.2 ± 0.4	14±1 ± 1
4.5	1.39±0.01 ± 0.03	2.46±0.04 ± 0.09	5.1±0.2 ± 0.4	12.1±0.9 ± 1.0
5.0	1.36±0.01 ± 0.03	2.33±0.04 ± 0.09	4.7±0.2 ± 0.4	10.7±0.7 ± 0.9
*	1.30±0.01 ± 0.03	2.08±0.03 ± 0.09	3.9±0.1 ± 0.3	8.2±0.5 ± 0.8
200 GeV				
η_c	F_2	F_3	F_4	F_5
0.2	1.51±0.04 ± 0.06	2.8±0.3 ± 0.3	6±2 ± 1	20±20 ± 10
0.25	1.50±0.04 ± 0.05	2.7±0.2 ± 0.3	6±2 ± 1	15±10 ± 10
0.5	1.50±0.02 ± 0.04	2.8±0.2 ± 0.3	6.1±0.9 ± 0.5	15±6 ± 5
1.0	1.47±0.02 ± 0.03	2.8±0.1 ± 0.2	6.1±0.5 ± 0.3	15±3 ± 1
1.5	1.43±0.01 ± 0.02	2.61±0.07 ± 0.16	5.6±0.3 ± 0.2	14±2 ± 1
2.0	1.40±0.01 ± 0.02	2.46±0.07 ± 0.10	5.1±0.3 ± 0.2	12±2 ± 1
2.5	1.36±0.01 ± 0.02	2.33±0.06 ± 0.07	4.7±0.3 ± 0.2	11±1 ± 1
3.0	1.33±0.01 ± 0.02	2.20±0.05 ± 0.06	4.3±0.2 ± 0.2	9.3±0.9 ± 0.5
3.5	1.30±0.01 ± 0.02	2.05±0.04 ± 0.06	3.7±0.2 ± 0.2	7.6±0.7 ± 0.5
4.0	1.27±0.01 ± 0.02	1.95±0.04 ± 0.06	3.5±0.1 ± 0.2	6.9±0.6 ± 0.5
4.5	1.25±0.01 ± 0.02	1.88±0.03 ± 0.06	3.2±0.1 ± 0.2	6.1±0.5 ± 0.5
5.0	1.24±0.01 ± 0.02	1.82±0.03 ± 0.06	3.0±0.1 ± 0.2	5.6±0.4 ± 0.5
*	1.21±0.01 ± 0.02	1.71±0.03 ± 0.06	2.7±0.1 ± 0.2	4.8±0.3 ± 0.5
900 GeV				
η_c	F_2	F_3	F_4	F_5
0.2	1.70±0.03 ± 0.02	4.2±0.2 ± 0.1	15±2 ± 1	80±10 ± 10
0.25	1.69±0.03 ± 0.02	4.2±0.2 ± 0.1	14±1 ± 1	50±10 ± 10
0.5	1.66±0.02 ± 0.02	3.9±0.2 ± 0.1	12±1 ± 1	43±9 ± 5
1.0	1.62±0.02 ± 0.01	3.7±0.1 ± 0.1	10.9±0.8 ± 0.1	40±5 ± 5
1.5	1.56±0.01 ± 0.01	3.30±0.09 ± 0.06	8.6±0.6 ± 0.1	26±4 ± 1
2.0	1.52±0.01 ± 0.01	3.07±0.08 ± 0.05	7.6±0.4 ± 0.1	22±3 ± 1
2.5	1.48±0.01 ± 0.01	2.88±0.07 ± 0.05	6.8±0.4 ± 0.1	18±2 ± 1
3.0	1.45±0.01 ± 0.01	2.74±0.06 ± 0.05	6.2±0.3 ± 0.1	16±2 ± 1
3.5	1.42±0.01 ± 0.01	2.57±0.05 ± 0.05	5.6±0.3 ± 0.1	14±1 ± 1
4.0	1.39±0.01 ± 0.01	2.44±0.04 ± 0.05	5.1±0.2 ± 0.1	11.9±0.8 ± 0.8
4.5	1.36±0.01 ± 0.01	2.32±0.04 ± 0.05	4.7±0.2 ± 0.1	10.6±0.9 ± 0.5
5.0	1.33±0.01 ± 0.01	2.21±0.04 ± 0.05	4.3±0.2 ± 0.1	9.3±0.7 ± 0.5
*	1.27±0.01 ± 0.01	1.97±0.03 ± 0.05	3.5±0.1 ± 0.1	7.1±0.4 ± 0.5

Table 3: The corrected charged particle multiplicity distributions given as probabilities in the central pseudorapidity intervals $|\eta| < 0.5, 1.5, 3.0$ and 5.0. The errors given contain both a statistical and a systematic component and are highly correlated between the bins. When the number of events per bin falls below 5, the bins are grouped and the entry represents the corresponding sum of the included bins.

$\|\eta\| < 0.5$			
200 GeV		900 GeV	
n	P_n	n	P_n
0	0.22±0.01	0	0.15±0.01
1	0.204±0.009	1	0.171±0.007
2	0.169±0.009	2	0.153±0.007
3	0.130±0.008	3	0.124±0.006
4	0.097±0.007	4	0.099±0.005
5	0.068±0.005	5	0.076±0.005
6	0.045±0.004	6	0.057±0.004
7	0.028±0.004	7	0.043±0.004
8	0.018±0.003	8	0.032±0.003
9	0.010±0.002	9	0.024±0.003
10	0.006±0.002	10	0.018±0.002
11	0.003±0.001	11	0.013±0.002
12	0.0017±0.0009	12	0.010±0.002
13-19	0.002±0.001	13	0.007±0.001
		14	0.005±0.001
		15	0.004±0.001
		16	0.0027±0.0009
		17	0.0021±0.0008
		18	0.0015±0.0007
		19	0.0011±0.0006
		20	0.0008±0.0005
		21-23	0.0013±0.0006
		24-31	0.0009±0.0005

continuation table 3

$\|\eta\| < 1.5$			
200 GeV		900 GeV	
n	P_n	n	P_n
0	0.045±0.006	0	0.033±0.006
1	0.060±0.005	1	0.035±0.005
2	0.063±0.005	2	0.048±0.004
3	0.072±0.006	3	0.058±0.004
4	0.080±0.006	4	0.065±0.004
5	0.083±0.006	5	0.066±0.004
6	0.080±0.006	6	0.063±0.004
7	0.073±0.006	7	0.060±0.004
8	0.067±0.005	8	0.056±0.004
9	0.058±0.005	9	0.051±0.004
10	0.050±0.005	10	0.046±0.004
11	0.042±0.004	11	0.042±0.003
12	0.036±0.004	12	0.038±0.003
13	0.031±0.004	13	0.034±0.003
14	0.026±0.003	14	0.031±0.003
15	0.022±0.003	15	0.028±0.003
16	0.019±0.003	16	0.025±0.003
17	0.016±0.003	17	0.023±0.003
18	0.014±0.002	18	0.021±0.002
19	0.011±0.002	19	0.018±0.002
20	0.010±0.002	20	0.017±0.002
21	0.008±0.002	21	0.015±0.002
22	0.007±0.002	22	0.014±0.002
23	0.006±0.002	23	0.012±0.002
24	0.005±0.001	24	0.011±0.002
25	0.004±0.001	25	0.010±0.002
26	0.003±0.001	26	0.009±0.002
27	0.002±0.001	27	0.008±0.002
28	0.0020±0.0009	28	0.007±0.001
29	0.0015±0.0008	29	0.007±0.001
30	0.0012±0.0007	30	0.006±0.001
31-32	0.0016±0.0009	31	0.005±0.001
33-45	0.0016±0.0008	32	0.005±0.001
		33	0.004±0.001
		34	0.004±0.001
		35	0.003±0.001
		36	0.0028±0.0009
		37	0.0025±0.0008
		38	0.0024±0.0008
		39	0.0019±0.0007
		40	0.0017±0.0007
		41	0.0014±0.0006
		42	0.0013±0.0006
		43	0.0011±0.0006
		44	0.0010±0.0005
		45	0.0009±0.0005
		46	0.0007±0.0005
		47-48	0.0012±0.0006
		49-50	0.0008±0.0005
		51-53	0.0008±0.0005
		54-58	0.0008±0.0005
		59-75	0.0007±0.0006

continuation table 3

$\|\eta\| < 3.0$			
200 GeV		900 GeV	
n	P_n	n	P_n
0	0.010±0.004	0	0.004±0.004
1	0.009±0.003	1	0.012±0.003
2	0.014±0.003	2	0.012±0.003
3	0.021±0.003	3	0.013±0.003
4	0.030±0.004	4	0.017±0.003
5	0.036±0.004	5	0.020±0.003
6	0.042±0.004	6	0.026±0.003
7	0.045±0.004	7	0.029±0.003
8	0.048±0.005	8	0.033±0.003
9	0.050±0.005	9	0.035±0.003
10	0.050±0.005	10	0.037±0.003
11	0.050±0.005	11	0.037±0.003
12	0.048±0.005	12	0.037±0.003
13	0.046±0.004	13	0.036±0.003
14	0.044±0.004	14	0.035±0.003
15	0.041±0.004	15	0.034±0.003
16	0.039±0.004	16	0.032±0.003
17	0.035±0.004	17	0.031±0.003
18	0.033±0.004	18	0.029±0.003
19	0.030±0.004	19	0.028±0.003
20	0.027±0.003	20	0.027±0.003
21	0.025±0.003	21	0.025±0.003
22	0.023±0.003	22	0.024±0.003
23	0.021±0.003	23	0.022±0.003
24	0.019±0.003	24	0.021±0.002
25	0.017±0.003	25	0.020±0.002
26	0.015±0.003	26	0.019±0.002
27	0.014±0.002	27	0.017±0.002
28	0.013±0.002	28	0.017±0.002
29	0.012±0.002	29	0.016±0.002
30	0.011±0.002	30	0.015±0.002
31	0.009±0.002	31	0.014±0.002
32	0.008±0.002	32	0.013±0.002
33	0.008±0.002	33	0.013±0.002
34	0.007±0.002	34	0.012±0.002
35	0.006±0.002	35	0.011±0.002
36	0.005±0.002	36	0.011±0.002
37	0.005±0.001	37	0.010±0.002
38	0.004±0.001	38	0.010±0.002
39	0.004±0.001	39	0.009±0.002
40	0.004±0.001	40	0.009±0.002
41	0.003±0.001	41	0.008±0.002

continuation table 3

$\|\eta\| < 3.0$			
200 GeV		900 GeV	
n	P_n	n	P_n
42	0.003±0.001	42	0.008±0.001
43	0.002±0.001	43	0.008±0.001
44	0.002±0.001	44	0.007±0.001
45	0.0018±0.0009	45	0.007±0.001
46	0.0016±0.0008	46	0.006±0.001
47	0.0015±0.0008	47	0.006±0.001
48	0.0013±0.0008	48	0.006±0.001
49-50	0.0020±0.0009	49	0.005±0.001
51-52	0.0015±0.0008	50	0.005±0.001
53-55	0.0013±0.0008	51	0.005±0.001
56-74	0.0014±0.0008	52	0.004±0.001
		53	0.004±0.001
		54	0.004±0.001
		55	0.004±0.001
		56	0.003±0.001
		57	0.003±0.001
		58	0.0030±0.0009
		59	0.0029±0.0009
		60	0.0026±0.0009
		61	0.0024±0.0008
		62	0.0022±0.0006
		63	0.0021±0.0006
		64	0.0019±0.0006
		65	0.0018±0.0006
		66	0.0017±0.0005
		67	0.0016±0.0005
		68	0.0014±0.0004
		69	0.0013±0.0004
		70	0.0013±0.0004
		71	0.0011±0.0004
		72	0.0011±0.0004
		73	0.0009±0.0004
		74	0.0008±0.0003
		75	0.0007±0.0003
		76-77	0.0013±0.0006
		78-79	0.0011±0.0006
		80-81	0.0009±0.0005
		82-84	0.0010±0.0005
		85-88	0.0010±0.0005
		89-95	0.0009±0.0005
		96-119	0.0009±0.0005

continuation table 3

$\|\eta\| < 5.0$			
200 GeV		900 GeV	
n	P_n	n	P_n
0- 2	0.01±0.01	0-2	0.0017±0.0007
3	0.008±0.003	3	0.003±0.001
4	0.010±0.003	4	0.006±0.002
5	0.013±0.003	5	0.005±0.003
6	0.019±0.003	6	0.008±0.003
7	0.023±0.003	7	0.008±0.003
8	0.028±0.004	8	0.013±0.002
9	0.032±0.004	9	0.012±0.002
10	0.034±0.004	10	0.015±0.002
11	0.039±0.004	11	0.017±0.002
12	0.039±0.004	12	0.022±0.002
13	0.040±0.004	13	0.022±0.003
14	0.043±0.004	14	0.023±0.003
15	0.042±0.004	15	0.026±0.003
16	0.042±0.004	16	0.026±0.003
17	0.040±0.004	17	0.028±0.003
18	0.039±0.004	18	0.029±0.003
19	0.038±0.004	19	0.028±0.003
20	0.036±0.004	20	0.028±0.003
21	0.034±0.004	21	0.028±0.003
22	0.032±0.004	22	0.027±0.003
23	0.030±0.004	23	0.026±0.003
24	0.028±0.004	24	0.026±0.003
25	0.026±0.003	25	0.025±0.003
26	0.024±0.003	26	0.024±0.003
27	0.022±0.003	27	0.023±0.003
28	0.021±0.003	28	0.022±0.003
29	0.019±0.003	29	0.021±0.002
30	0.018±0.003	30	0.020±0.002
31	0.016±0.003	31	0.019±0.002
32	0.015±0.003	32	0.018±0.002
33	0.014±0.002	33	0.018±0.002
34	0.013±0.002	34	0.017±0.002
35	0.012±0.002	35	0.016±0.002
36	0.011±0.002	36	0.015±0.002
37	0.009±0.002	37	0.015±0.002
38	0.009±0.002	38	0.014±0.002
39	0.008±0.002	39	0.014±0.002
40	0.008±0.002	40	0.013±0.002
41	0.007±0.002	41	0.013±0.002
42	0.006±0.002	42	0.012±0.002
43	0.005±0.002	43	0.011±0.002
44	0.005±0.001	44	0.011±0.002
45	0.005±0.001	45	0.011±0.002
46	0.004±0.001	46	0.011±0.002
47	0.004±0.001	47	0.010±0.002
48	0.003±0.001	48	0.010±0.002
49	0.003±0.001	49	0.009±0.002
50	0.002±0.001	50	0.009±0.002
51	0.002±0.001	51	0.008±0.002
52	0.0019±0.0009	52	0.008±0.002

continuation table 3

$\|\eta\| < 5.0$			
200 GeV		900 GeV	
n	P_n	n	P_n
53	0.0016±0.0008	53	0.008±0.002
54	0.0015±0.0008	54	0.008±0.001
55	0.0013±0.0008	55	0.007±0.001
56-57	0.0019±0.0009	56	0.007±0.001
58-59	0.0013±0.0008	57	0.007±0.001
60-62	0.0012±0.0007	58	0.007±0.001
63-77	0.0013±0.0007	59	0.006±0.001
		60	0.006±0.001
		61	0.006±0.001
		62	0.006±0.001
		63	0.005±0.001
		64	0.005±0.001
		65	0.005±0.001
		66	0.005±0.001
		67	0.005±0.001
		68	0.004±0.001
		69	0.004±0.001
		70	0.004±0.001
		71	0.004±0.001
		72	0.003±0.001
		73	0.004±0.001
		74	0.003±0.001
		75	0.0028±0.0009
		76	0.0027±0.0009
		77	0.0025±0.0009
		78	0.0024±0.0008
		79	0.0022±0.0008
		80	0.0020±0.0008
		81	0.0019±0.0007
		82	0.0019±0.0007
		83	0.0016±0.0007
		84	0.0016±0.0007
		85	0.0014±0.0006
		86	0.0014±0.0006
		87	0.0013±0.0006
		88	0.0011±0.0006
		89	0.0011±0.0006
		90	0.0009±0.0005
		91	0.0009±0.0005
		92	0.0008±0.0005
		93	0.0008±0.0005
		94	0.0008±0.0005
		95-96	0.0012±0.0006
		97-98	0.00011±0.0006
		99-100	0.0009±0.0005
		101-102	0.0008±0.0005
		103-106	0.0011±0.0006
		107-111	0.0009±0.0005
		112-118	0.0007±0.0005
		119-137	0.0008±0.0005

Table 4: Moments of the corrected multiplicity distributions in non-centred intervals of pseudorapidity. The errors given are statistical only. Systematic error are estimated to be of the same magnitude as the systematic errors in the data for the central pseudorapidity interval $\eta_c = 0.5$.

200 GeV							
$\|\eta\|$-interval	$< n >$	D_2	$< n > / D_2$	C_2	C_3	C_4	C_5
0.0-1.0	2.59±0.03	2.50±0.02	1.04±0.01	1.93±0.02	5.0±0.1	16±1	60±9
0.5-1.5	2.70±0.03	2.56±0.02	1.06±0.01	1.90±0.02	4.9±0.1	16±1	59±8
1.0-2.0	2.73±0.03	2.52±0.02	1.08±0.01	1.85±0.02	4.6±0.1	13.9±0.9	50±7
1.5-2.5	2.62±0.03	2.44±0.02	1.08±0.01	1.87±0.02	4.7±0.1	14.3±0.9	51±7
2.0-3.0	2.41±0.02	2.34±0.02	1.03±0.01	1.95±0.02	5.3±0.1	19.2±0.9	85±7
2.5-3.5	2.12±0.02	2.02±0.02	1.05±0.01	1.90±0.02	4.8±0.1	15.0±0.9	54±7
>0	10.5±0.05	6.33±0.04	1.64±0.01	1.36±0.01	2.35±0.02	4.36±0.07	9.5±0.4
900 GeV							
$\|\eta\|$-interval	$< n >$	D_2	$< n > / D_2$	C_2	C_3	C_4	C_5
0.0-1.0	3.68±0.04	3.61±0.03	1.02±0.01	1.96±0.02	5.4±0.2	19±1	80±10
0.5-1.5	3.76±0.04	3.56±0.03	1.06±0.01	1.90±0.02	5.0±0.1	17±1	67±8
1.0-2.0	3.82±0.04	3.50±0.03	1.09±0.01	1.84±0.02	4.6±0.1	14.5±0.8	54±6
1.5-2.5	3.79±0.04	3.41±0.03	1.11±0.01	1.81±0.01	4.4±0.1	13.3±0.7	46±5
2.0-3.0	3.59±0.04	3.20±0.03	1.12±0.01	1.80±0.01	4.36±0.09	13.1±0.6	46±4
2.5-3.5	3.34±0.04	2.95±0.03	1.13±0.01	1.78±0.01	4.25±0.09	12.5±0.6	43±4
>0	17.7±0.1	10.9±0.1	1.63±0.01	1.38±0.01	2.37±0.02	4.8±0.1	11.0±0.4

Table 5: Results of fitting the negative binomial distribution with the parameters $\overline{n}$ and k to the multiplicity distributions in central intervals of pseudorapidity, defined by $|\eta| < \eta_c$ and in full phase space (denoted with $*$) at 200 and 900 GeV. The value of χ_0^2 and the number of degrees of freedom (NDF) are given and the corresponding probability $P(\chi^2 > \chi_0^2)$.

200 GeV				
η_c	$\overline{n}$	k	χ_0^2/NDF	Prob.
0.2	0.96±0.02	1.8±0.2±0.2	9/4	6%
0.25	1.21±0.03	1.9±0.2±0.2	14/6	3%
0.5	2.48±0.06	2.0±0.2±0.1	28/10	0.2%
1.0	5.32±0.08	2.3±0.2±0.1	21/17	23%
1.5	8.1±0.1	2.6±0.1±0.1	25/23	34%
2.0	10.7±0.1	2.6±0.1±0.1	34/30	28%
2.5	13.2±0.1	2.8±0.1±0.1	51/34	3%
3.0	15.4±0.2	3.1±0.1±0.1	60/39	2%
3.5	17.4±0.1	3.4±0.1±0.1	52/41	12%
4.0	18.8±0.2	3.7±0.1±0.1	49/43	25%
4.5	19.8±0.1	4.1±0.1±0.1	56/44	11%
5.0	20.4±0.2	4.3±0.1±0.2	49/45	17%
*	21.2±0.2	4.8±0.2±0.2	50/43	21%
900 GeV				
η_c	$\overline{n}$	k	χ_0^2/NDF	Prob.
0.2	1.42±0.02	1.5±0.1±0.1	6/8	65%
0.25	1.79±0.03	1.5±0.1±0.1	10/9	32%
0.5	3.55±0.07	1.5±0.1±0.1	14/15	53%
1.0	7.4±0.1	1.7±0.1±0.1	31/28	32%
1.5	11.1±0.1	1.8±0.1±0.1	66/37	0.3%
2.0	15.0±0.2	2.0±0.1±0.1	74/48	0.9%
2.5	18.8±0.2	2.1±0.1±0.1	84/57	1%
3.0	22.2±0.2	2.3±0.1±0.1	109/63	0.03%
3.5	25.3±0.2	2.4±0.1±0.1	127/68	0.02%
4.0	28.0±0.3	2.6±0.1±0.1	133/70	0.01%
4.5	30.3±0.3	2.9±0.1±0.1	153/73	10^{-7}
5.0	32.2±0.3	3.1±0.1±0.2	151/75	10^{-7}
*	35.2±0.3	3.7±0.1±0.2	160/73	10^{-8}

Table 6: Results of fitting the negative binomial distribution with the parameters $\overline{n}$ and k to the multiplicity distributions in non-central intervals of pseudorapidity at 200 and 900 GeV c.m. energy. The value of χ_0^2 and the number of degrees of freedom (NDF) are given and the corresponding probability.

200 GeV				
$\|\eta\|$-interval	$\overline{n}$	k	χ_0^2/NDF	Prob.
0.0-1.0	2.58±0.03	1.79±0.07±0.10	30/11	0.2%
0.5-1.5	2.70±0.03	1.85±0.07±0.10	19/12	9%
1.0-2.0	2.73±0.03	1.95±0.08±0.10	18/11	8%
1.5-2.5	2.62±0.03	1.99±0.08±0.10	16/10	10%
2.0-3.0	2.40±0.03	2.01±0.07±0.10	22/9	0.6%
2.5-3.5	2.14±0.03	2.2±0.1±0.1	18/7	1%
> 0.0	10.6±0.1	4.0±0.1±0.1	32/25	16%
900 GeV				
$\|\eta\|$-interval	$\overline{n}$	k	χ_0^2/NDF	Prob.
0.0-1.0	3.68±0.05	1.48±0.06±0.10	21/18	28%
0.5-1.5	3.82±0.05	1.66±0.07±0.10	26/17	7%
1.0-2.0	3.90±0.05	1.81±0.07±0.10	22/16	14%
1.5-2.5	3.88±0.05	1.95±0.08±0.10	22/15	11%
2.0-3.0	3.72±0.05	2.2±0.1±0.1	20/13	10%
2.5-3.5	3.41±0.05	2.2±0.1±0.1	12/11	36%
> 0.0	17.6±0.1	3.3±0.1±0.1	83/41	10^{-4}

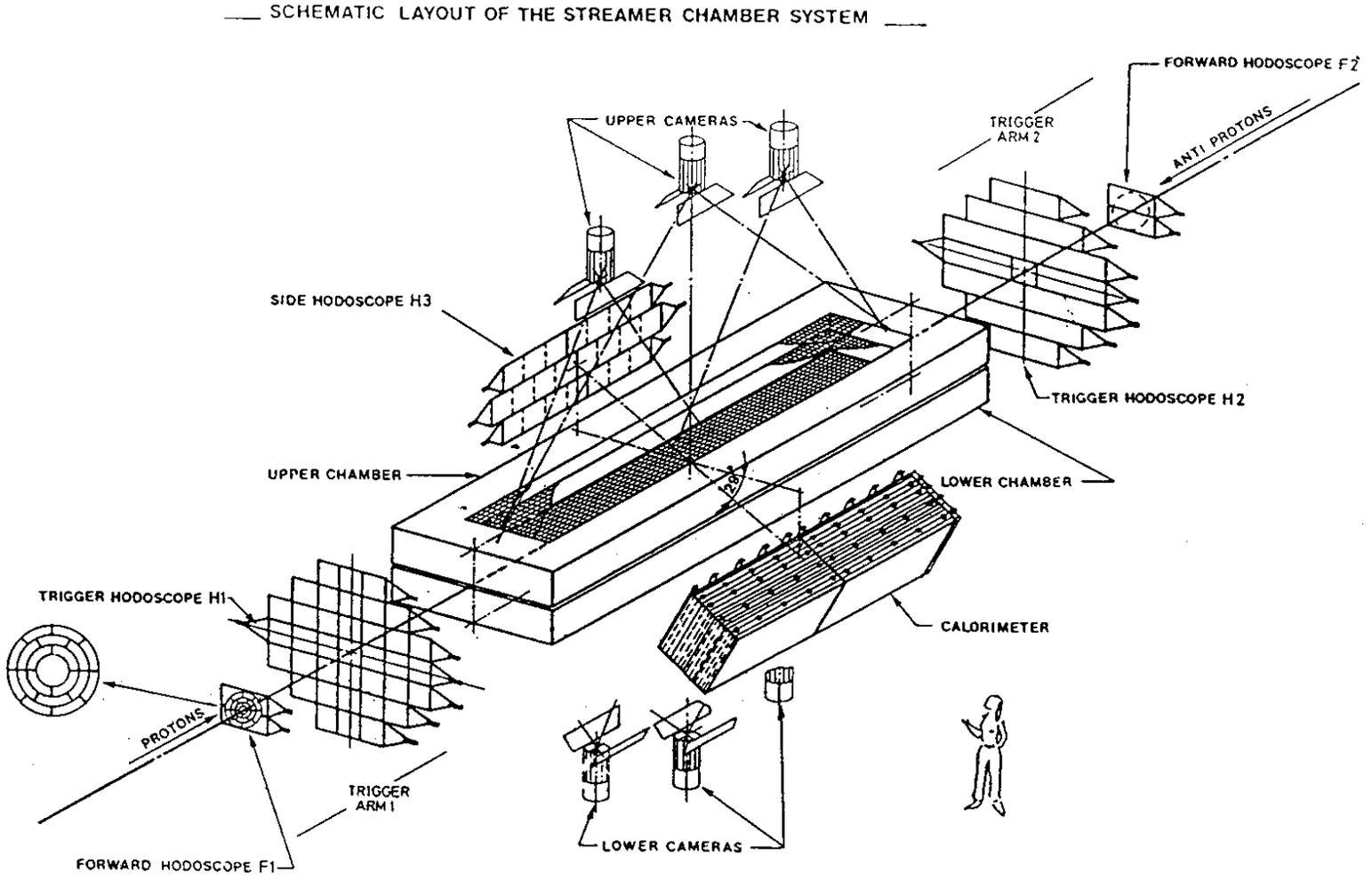

Figure 1: The UA5 detector.

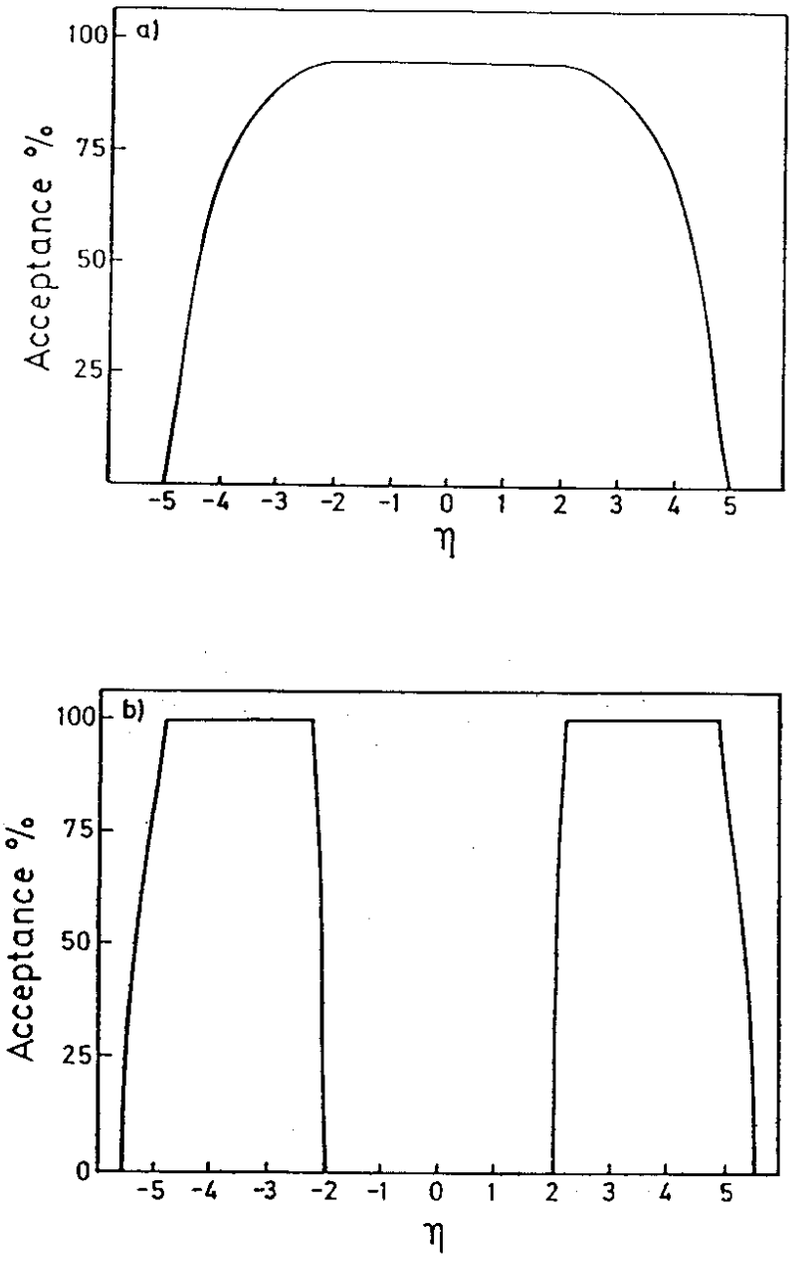

Figure 2: a) The geometrical acceptance of the streamer chambers. b) The acceptance of the trigger hodoscopes.

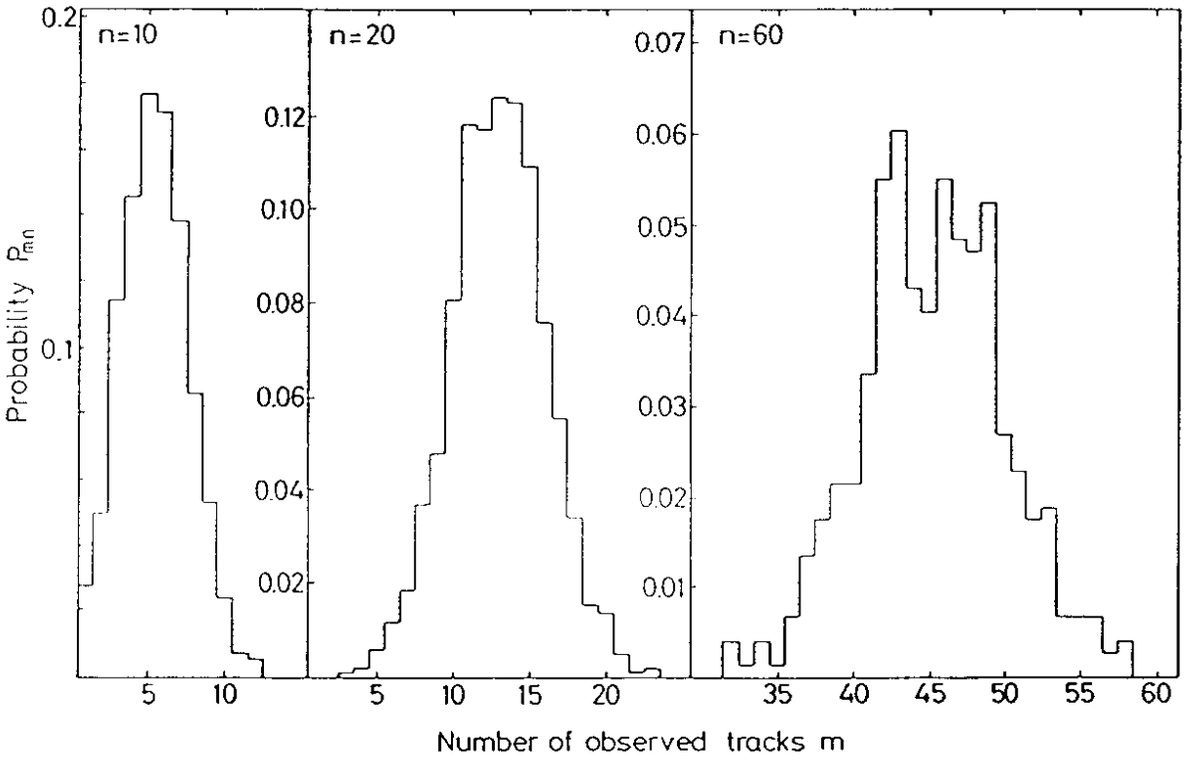

Figure 3: The observed multiplicity distributions P_{mn} for true multiplicities fixed at n =10, 20, and 60, respectively, as estimated with the UA5 Monte Carlo simulation program for 900 GeV full phase space.

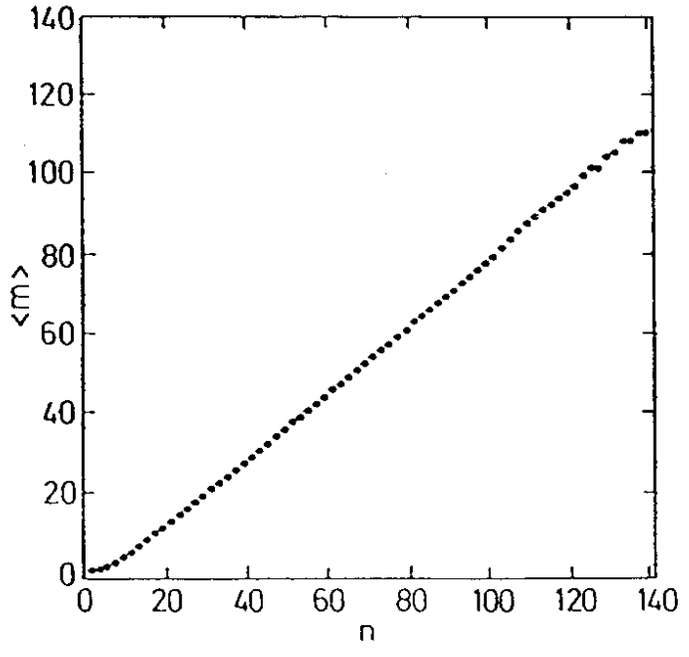

Figure 4: The mean of the observed distribution versus the true number of particles at 900 GeV full phase space, as simulated with the UA5 Monte Carlo program.

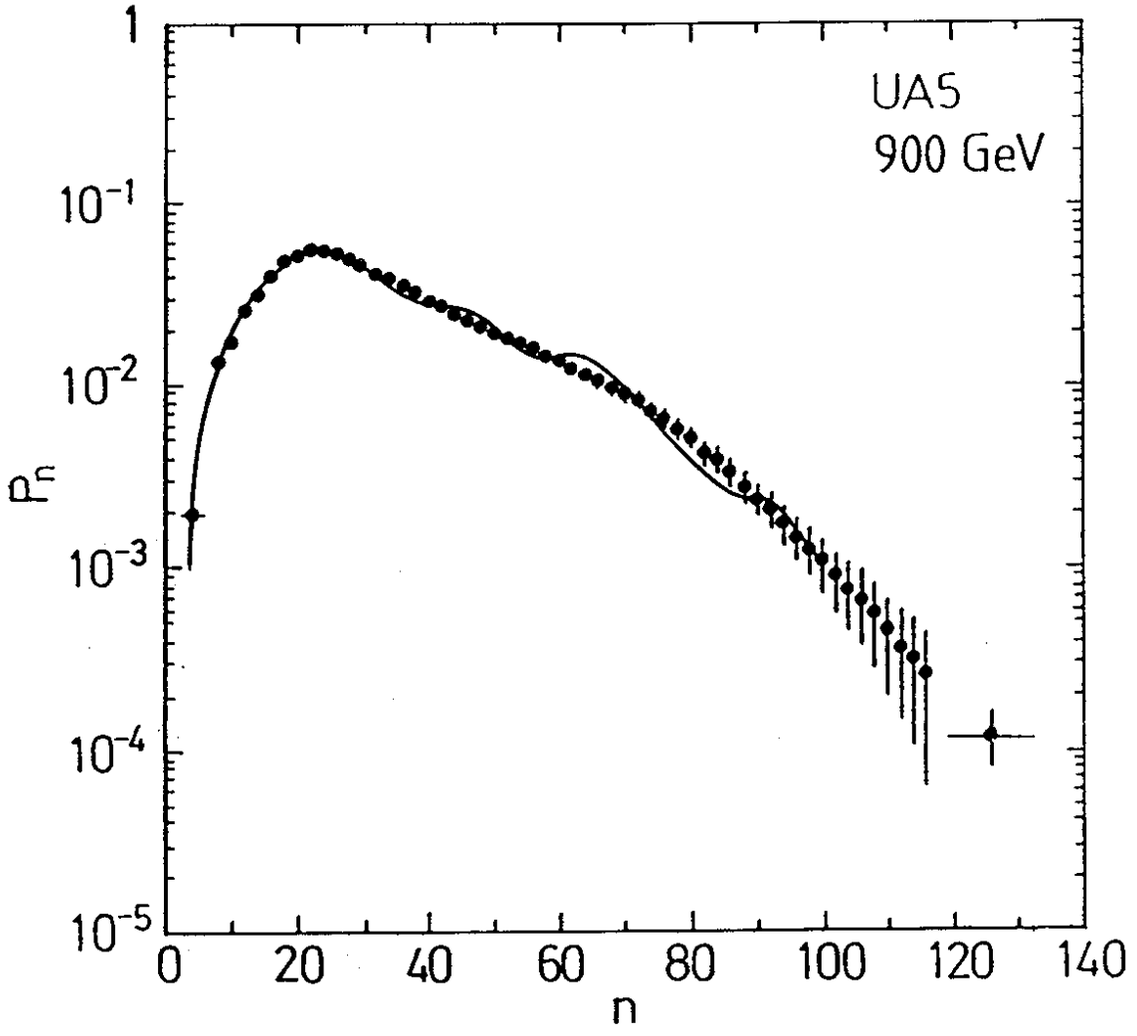

Figure 5: The true multiplicity distribution for non single-diffractive $\bar{p}p$-collisions at 900 GeV in full phase space derived by the two different methods described in the text. The points were obtained by the method of maximum entropy, the line by the iterative method.

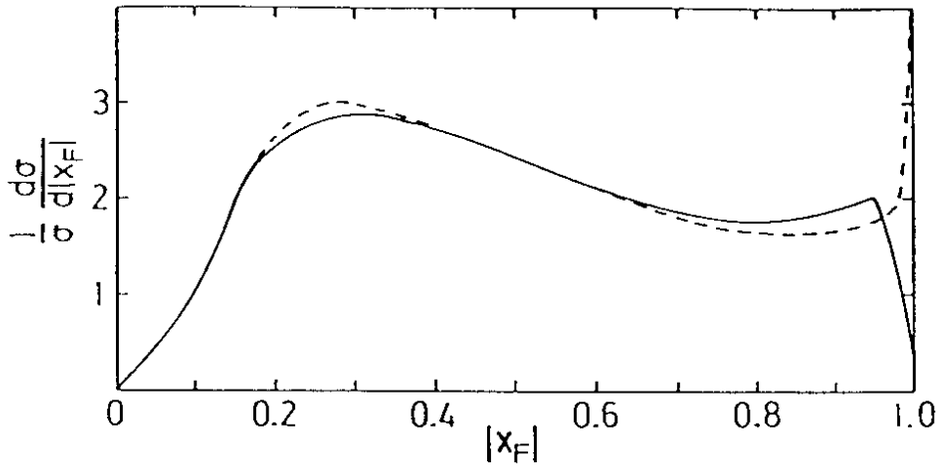

Figure 6: The Feynman-x distribution for leading baryons for two different options in the UA5 event generator program. The full line shows the case for which large values of $|x_F|$ have been suppressed and the dashed line the distribution without this suppression.

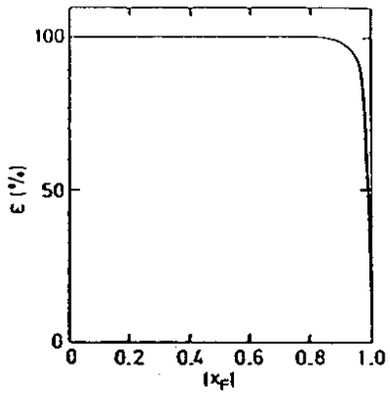

Figure 7: The trigger efficiency in one trigger arm as a function of $|x_F|$ of the leading baryon on the same side.

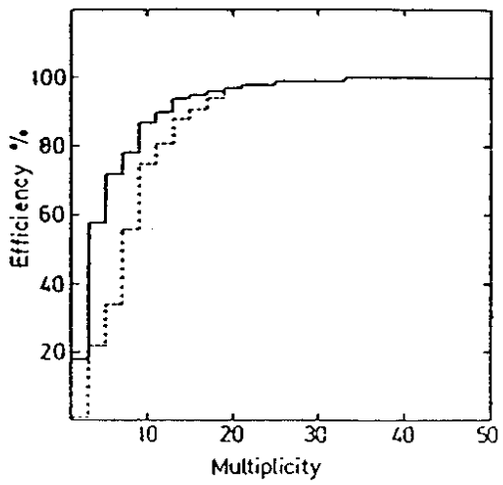

Figure 8: The trigger efficiency at 900 GeV full phase space for two different x_F-distributions of the leading baryons. The full line represents the case with suppression of large value of $|x_F|$, the dotted line the case without suppression.

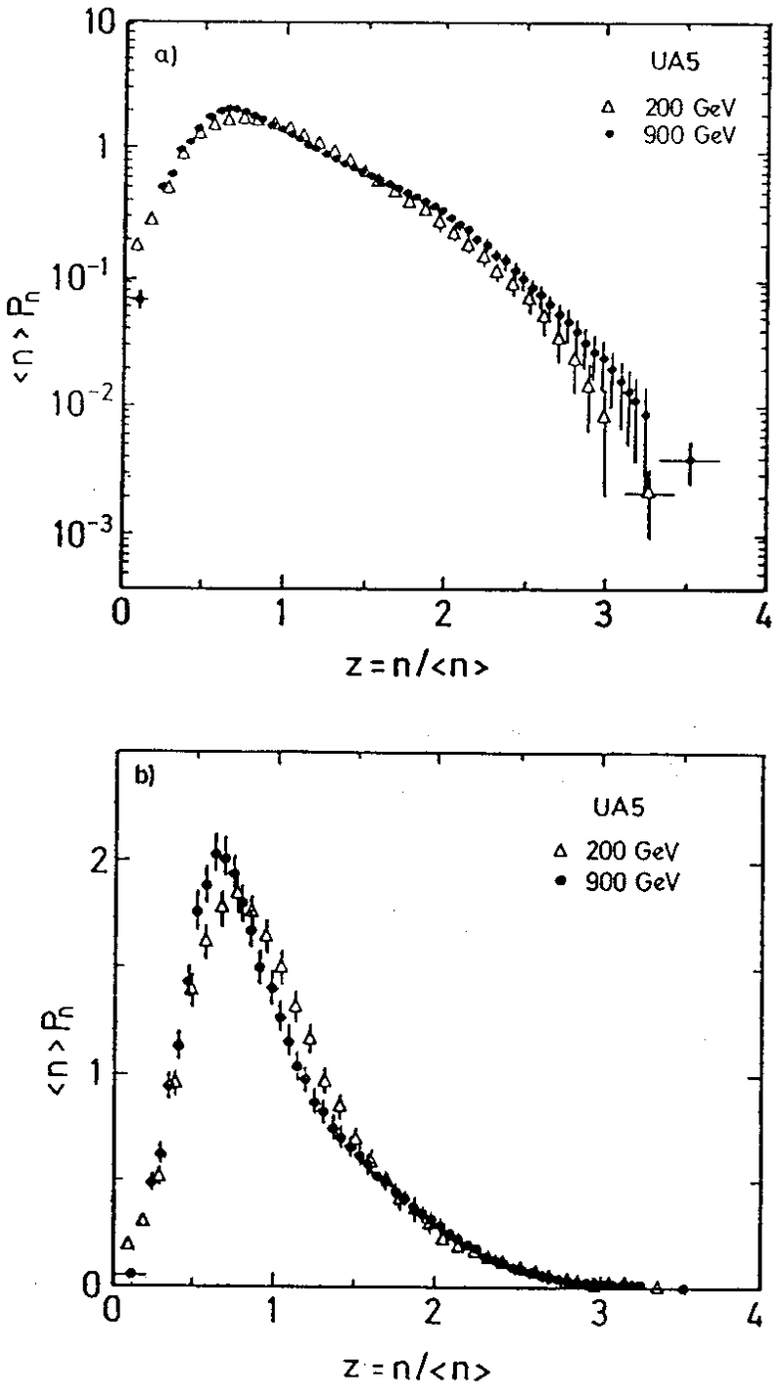

Figure 9: The multiplicity distributions for inelastic, non single-diffractive events at 200 and 900 GeV in full phase space in KNO variables, a) logarithmic scale, b) linear probability scale.

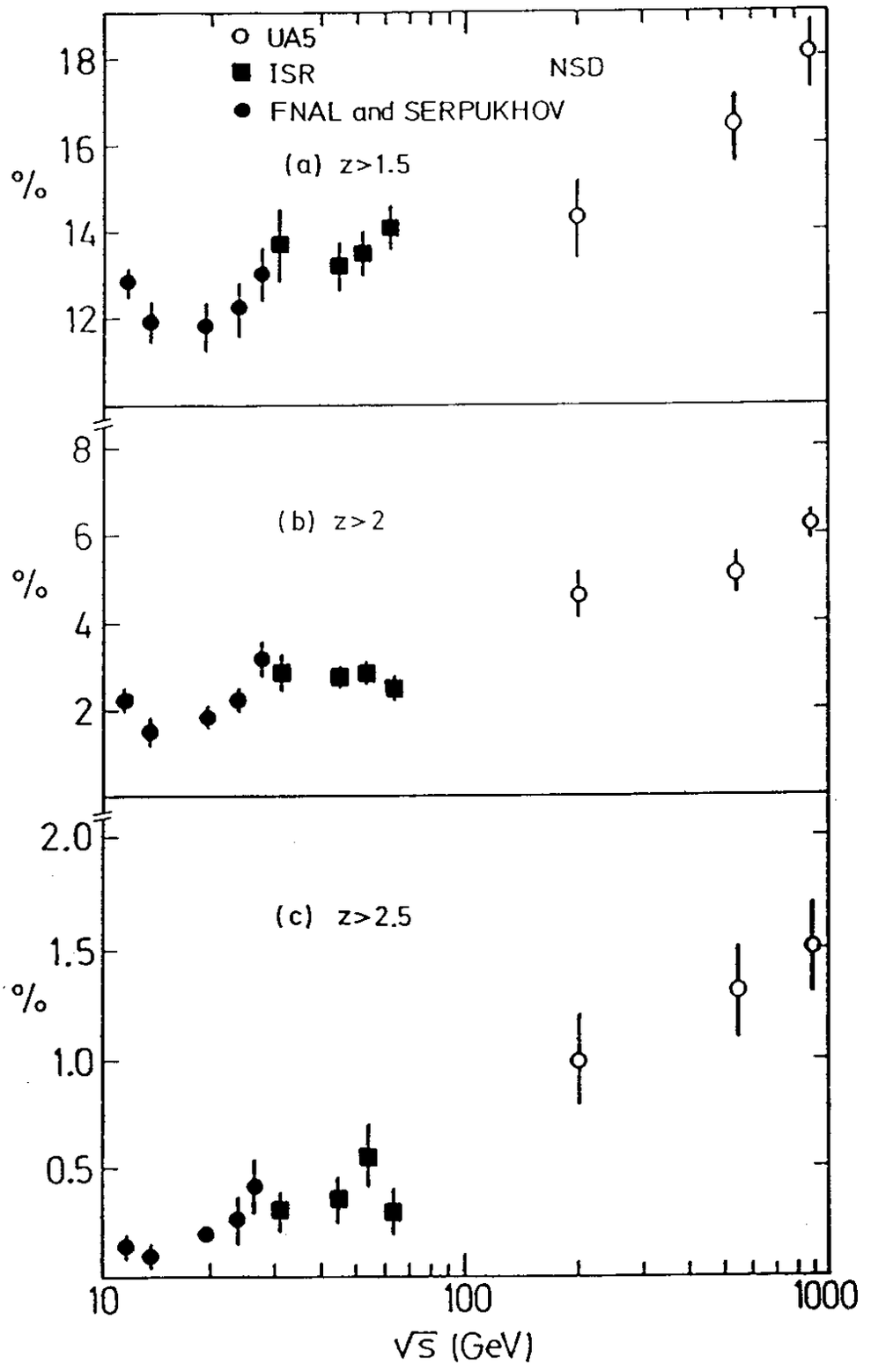

Figure 10: The percentage of events in the high multiplicity tail for (a) $z > 1.5$, (b) $z > 2.0$ and (c) $z > 2.5$ as a function of the centre of mass energy. The values from Serpukhov, FNAL and ISR were calculated from results given in ref. [1,2,3] and the values at 546 GeV are given in ref [15].

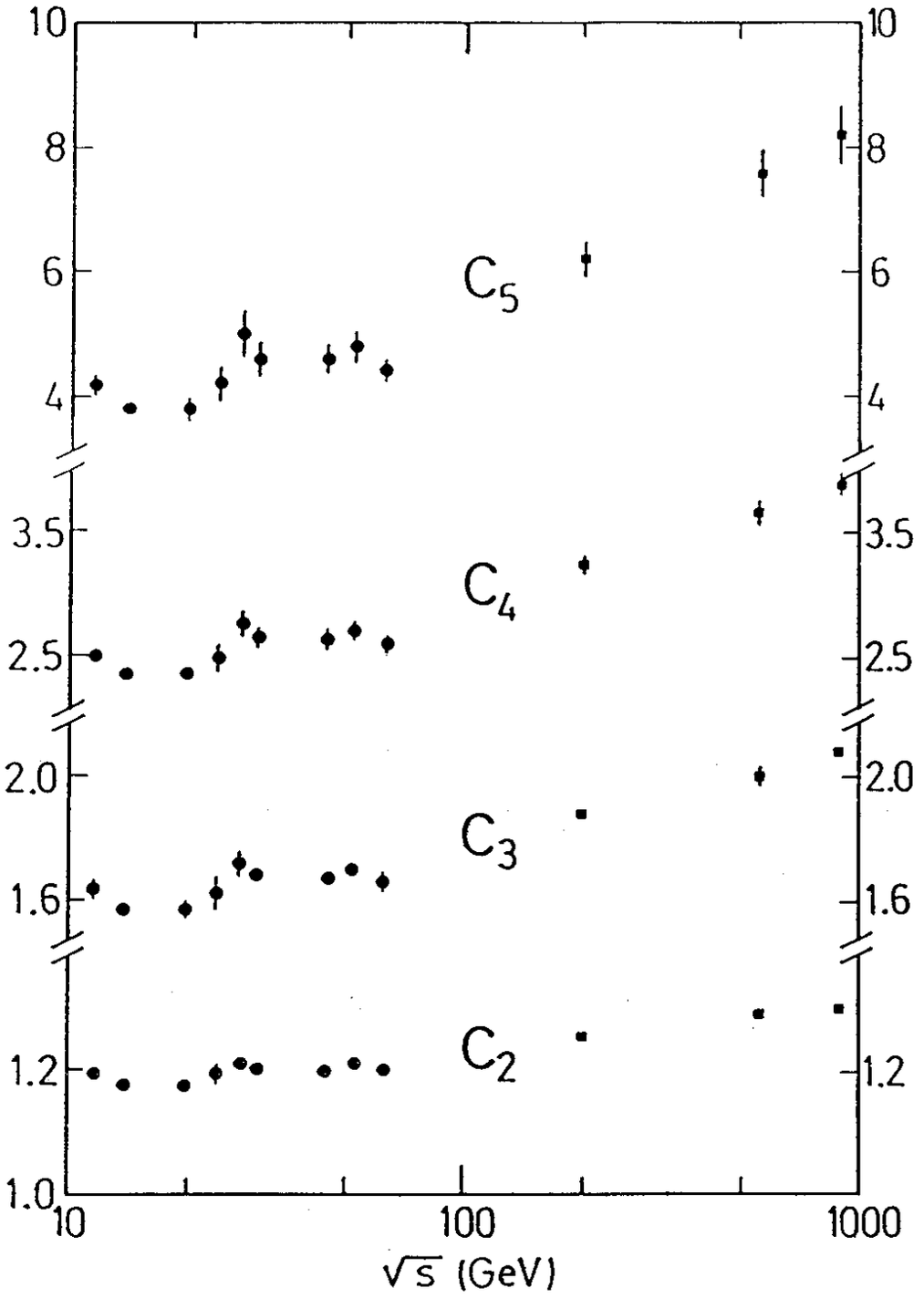

Figure 11: Values of the first four C-moments for the non single-diffractive distributions as a function of the centre of mass energy. The circles show Serpukhov, FNAL and ISR [1,2,3] data and the squares UA5 data. The values at 546 GeV are given in ref. [15].

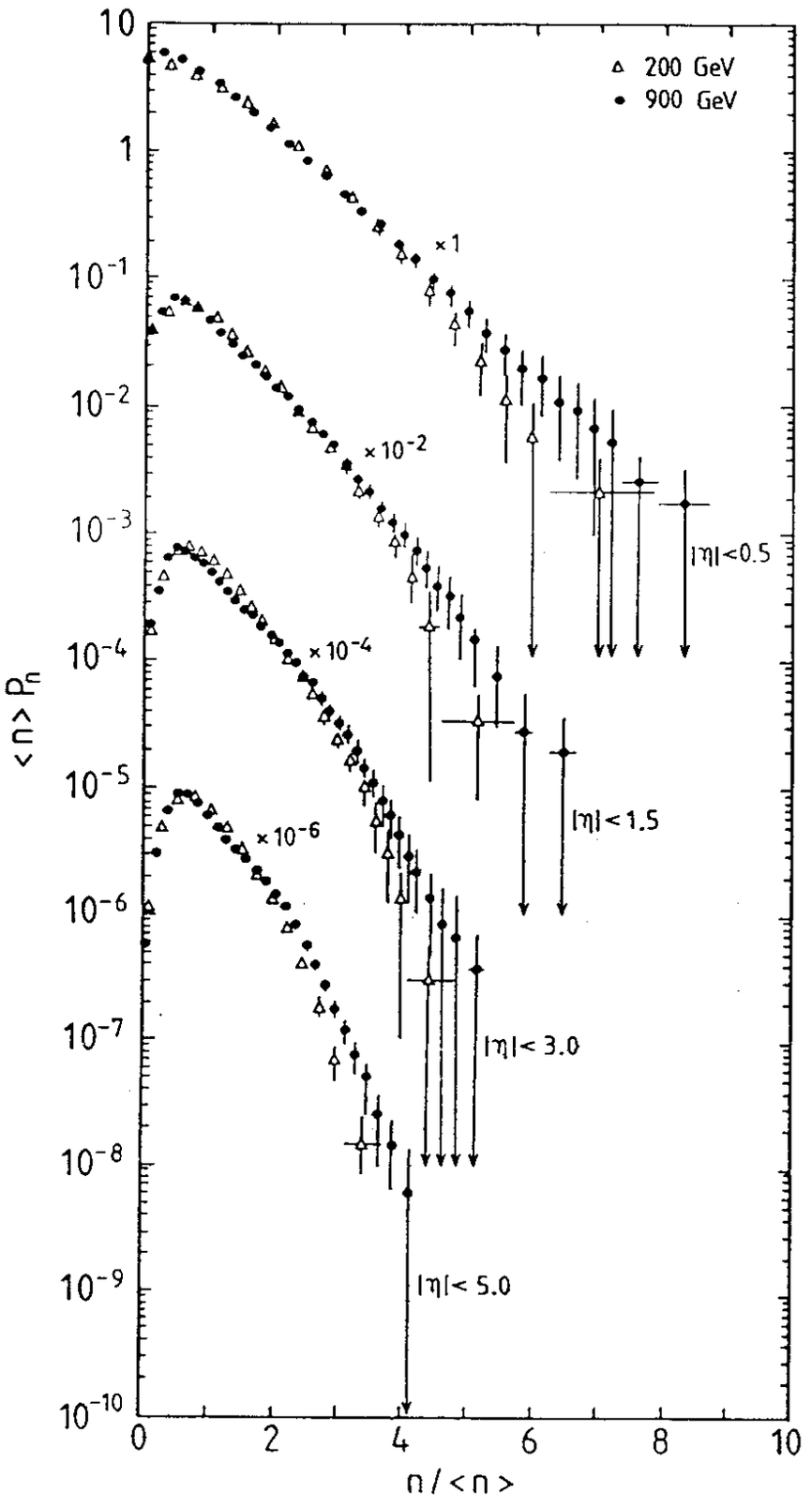

Figure 12: Charged particle multiplicity distributions in limited intervals of pseudorapidity at centre of mass energies of 200 and 900 GeV.

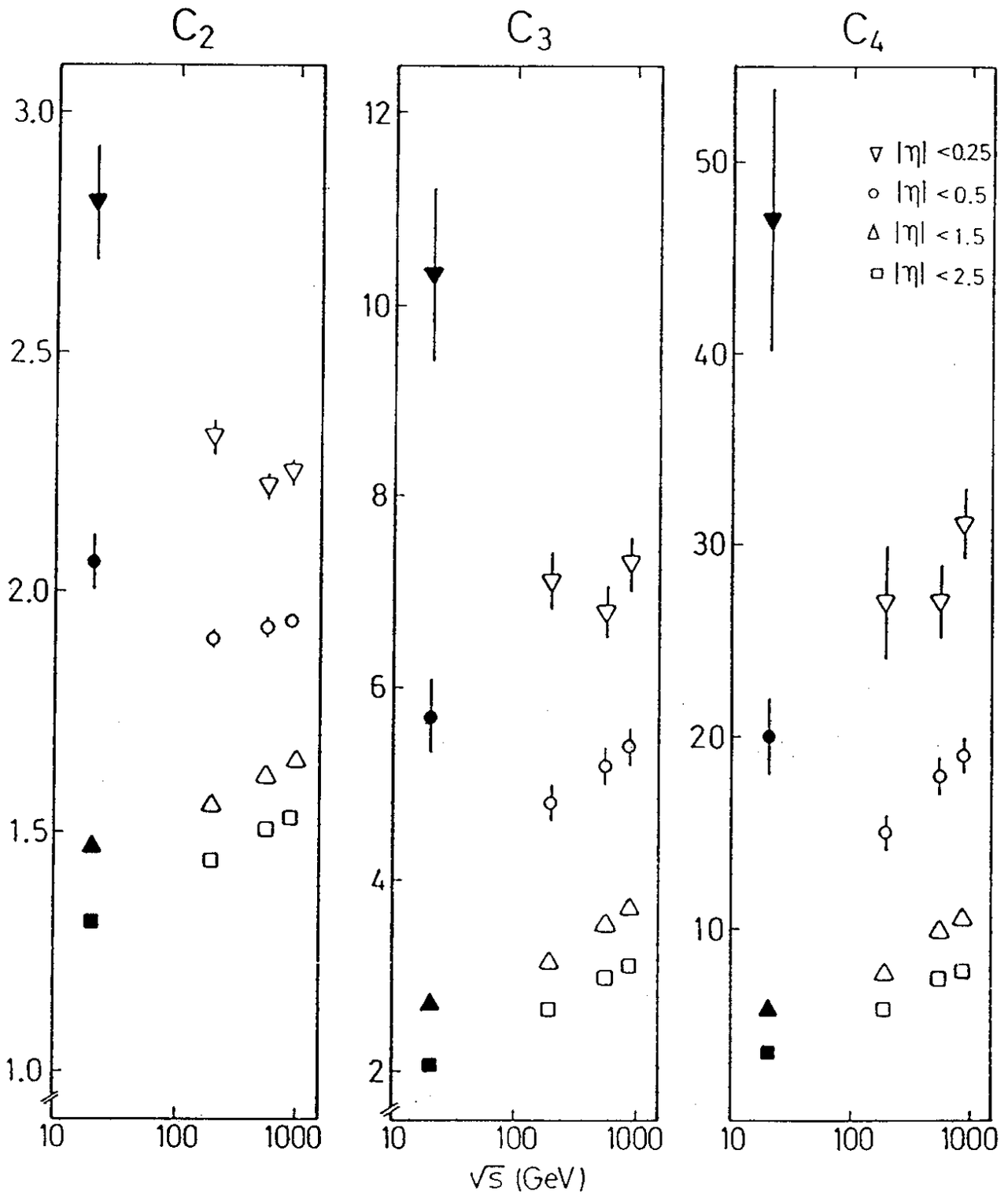

Figure 13: The C-moments for the charged particle multiplicity distributions in four selected intervals of pseudorapidity plotted versus the centre of mass energy. The filled points show NA22 data [26] and the open points UA5 data. The values at 546 GeV are taken from ref. [7].

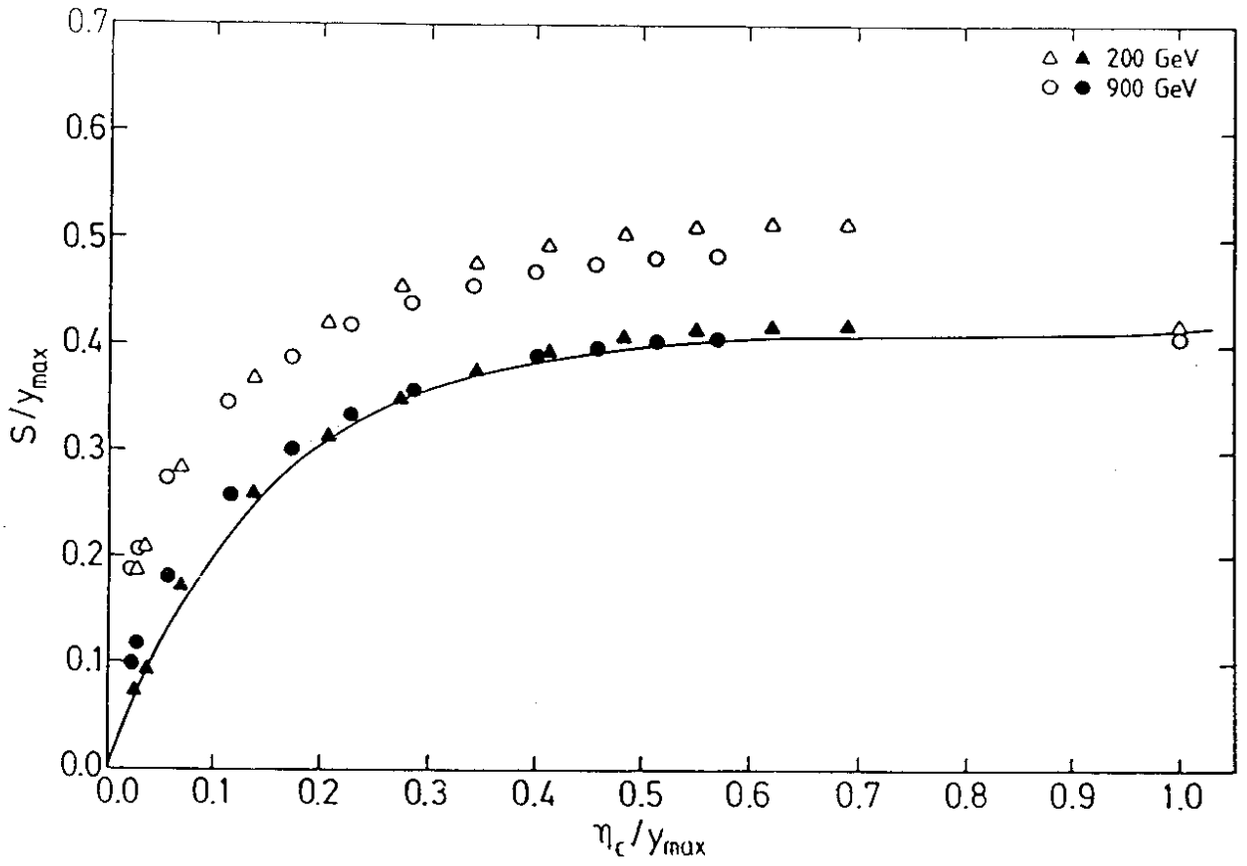

Figure 14: The scaled entropy S/y_{max} versus the scaled pseudorapidity, η_c/y_{max} for the 200 and 900 GeV data. The open symbols represent data points for all multiplicities whereas the filled symbols represent even multiplicities only. The errors on the experimental points are within the plotted symbols. The curve for S(even n) is taken from ref. [25].

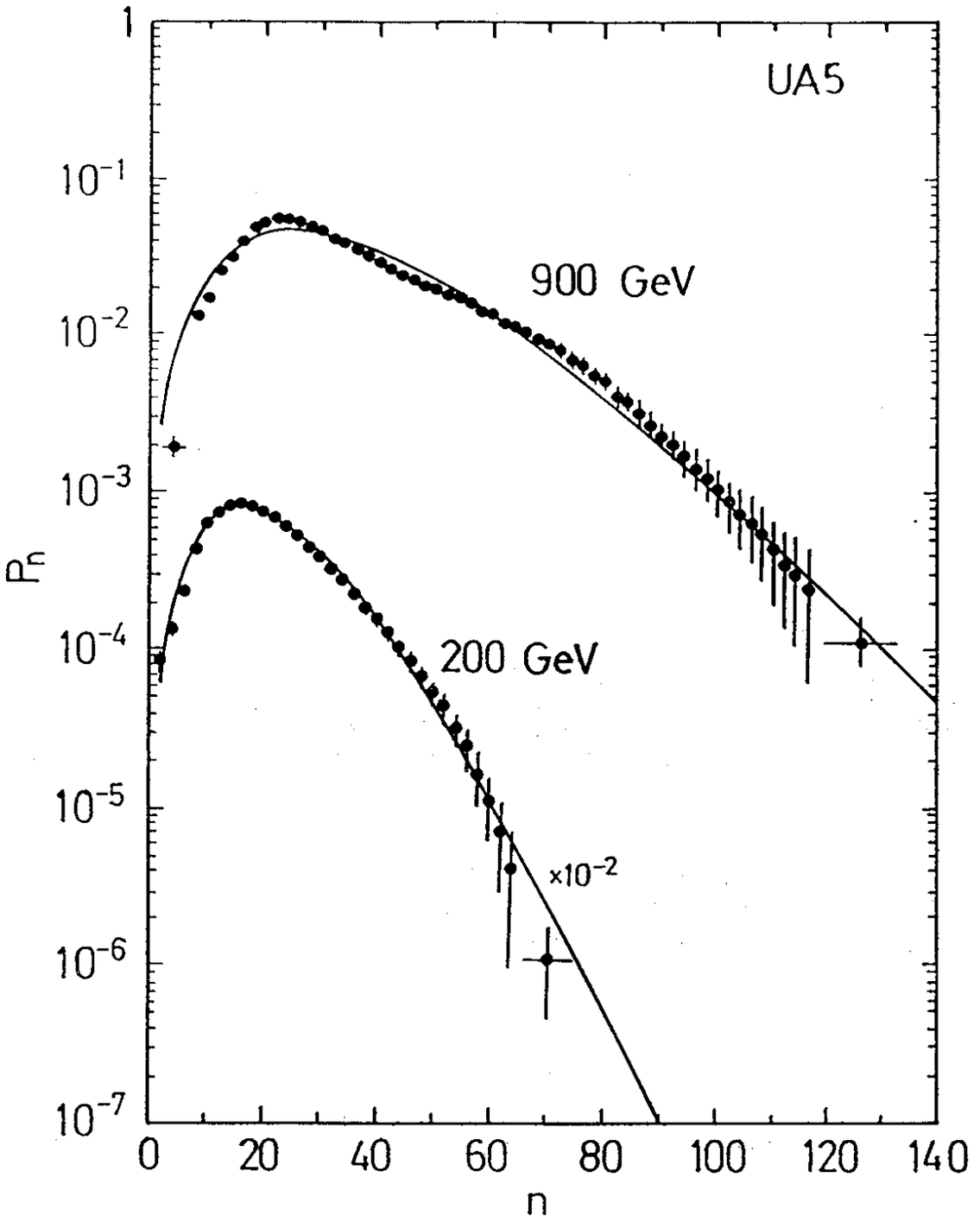

Figure 15: The best fitted negative binomial distribution compared to the true multiplicity distribution in full phase space at 200 and 900 GeV centre of mass energies. The points are data points taken from table 1, the lines connect points of the negative binomial distributions.

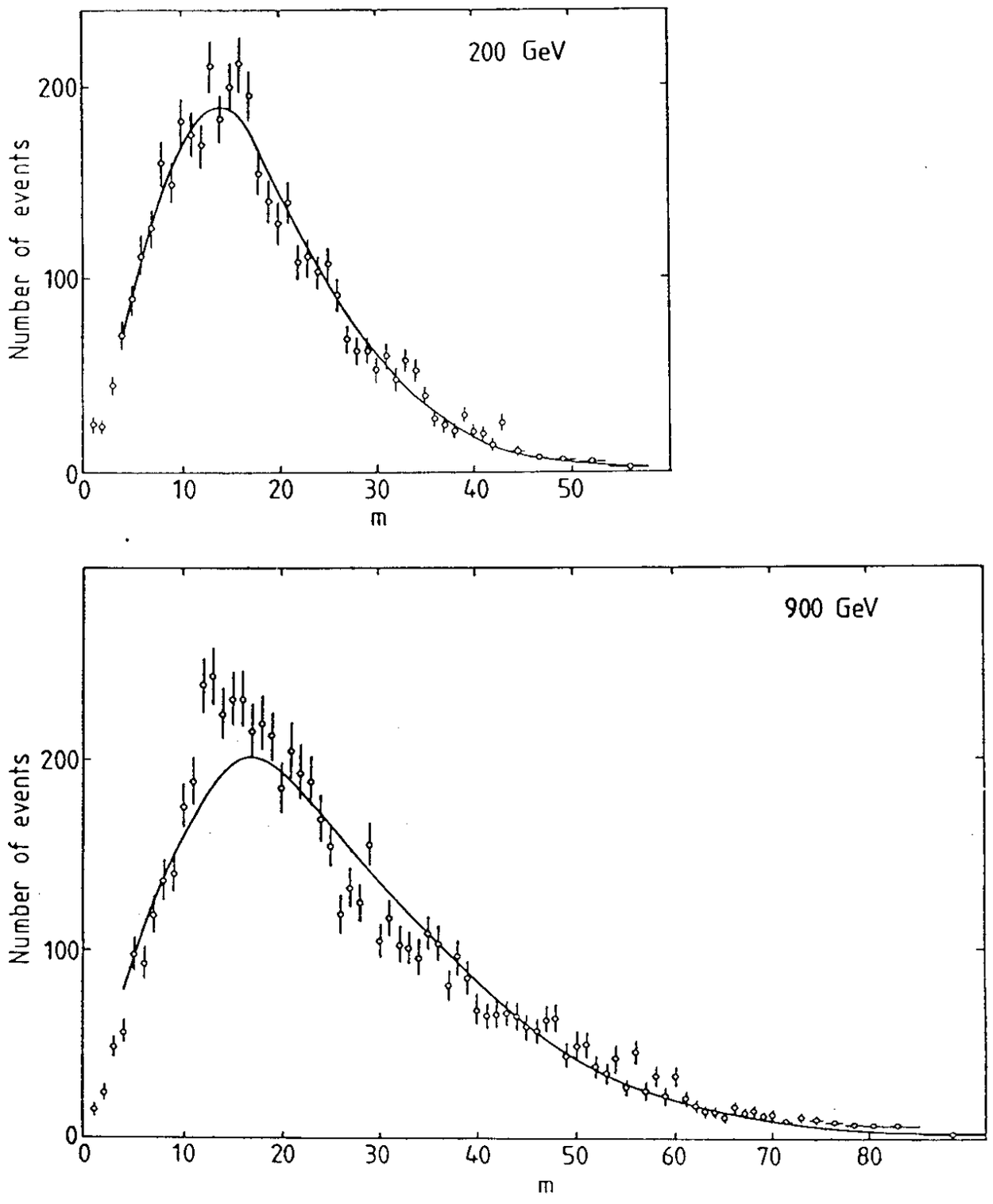

Figure 16: The best fitted negative binomial distribution compared to the observed multiplicity distributions in full phase space at 200 and 900 GeV centre of mass energies. The points represent data and the lines connect points of the negative binomial distributions.

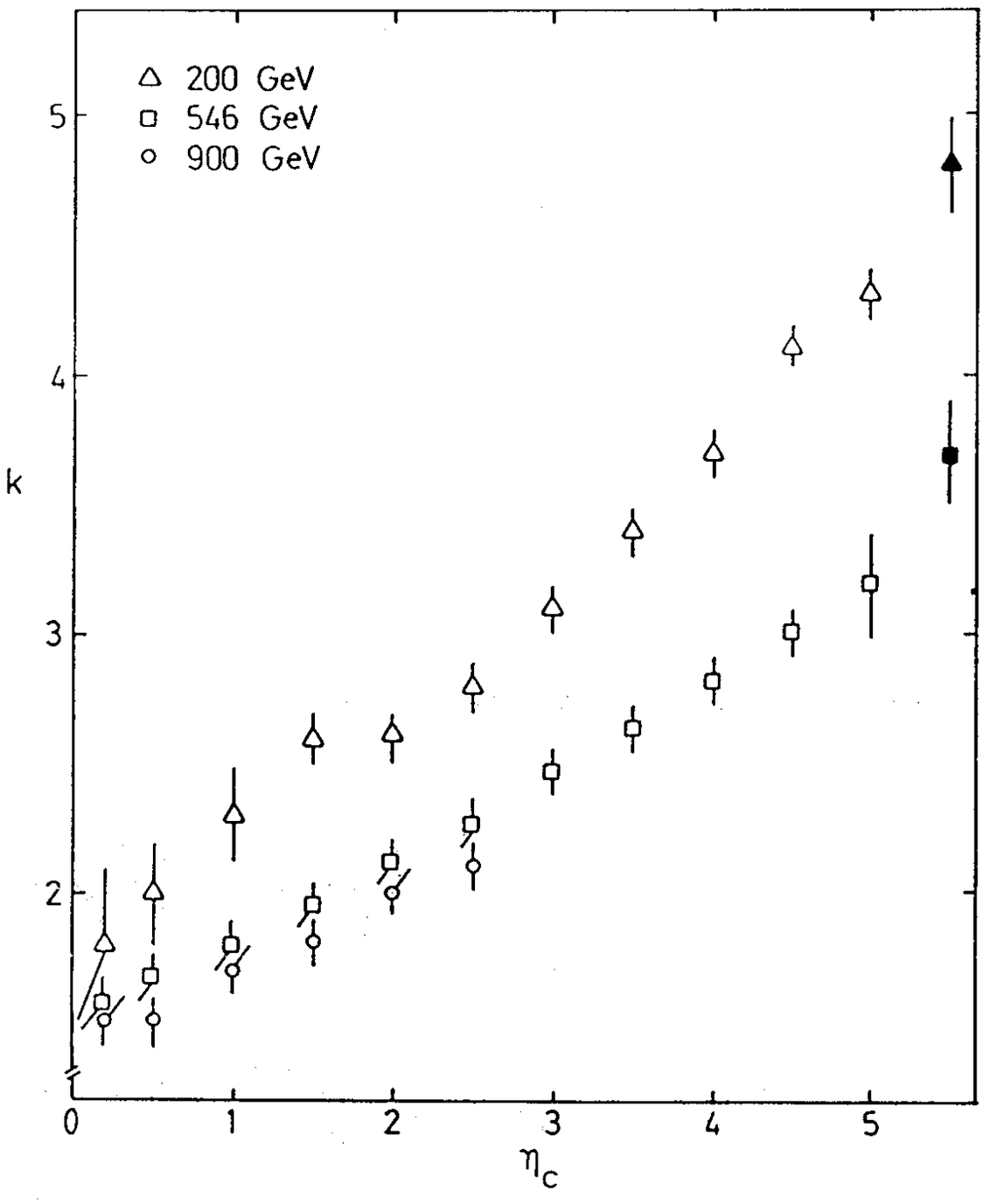

Figure 17: The negative binomial parameter k plotted as a function of the size of the central pseudorapidity interval defined by $|\eta| < \eta_c$. At 900 GeV only those k values are plotted which represent acceptable fits.

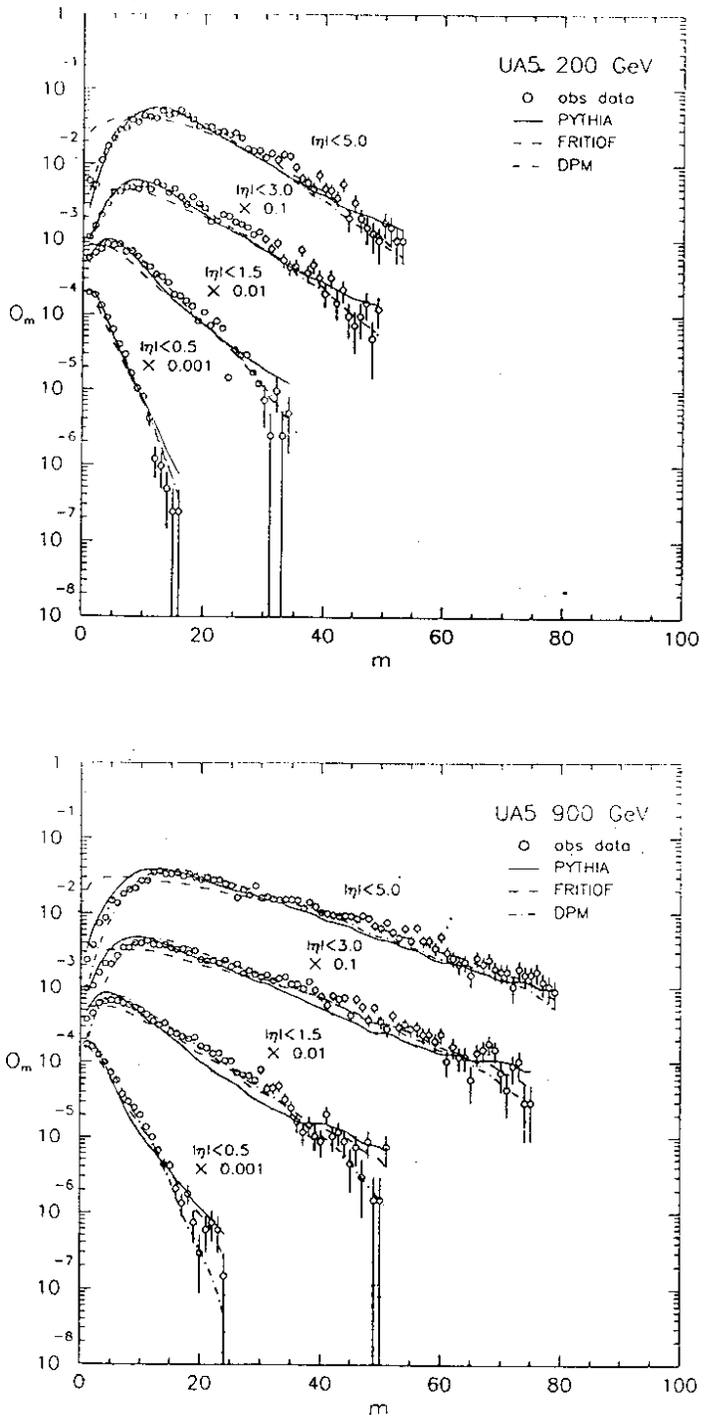

Figure 18: The predictions of the three models compared with the observed distributions at 200 and 900 GeV c.m. energies in limited intervals of pseudorapidity. The models are the Pythia, the Fritiof and the Dual Parton model. The distribution of a model, F_n, has been transformed to a predicted observed distribution by $O_m = \sum_n P_{mn}\epsilon_n F_n$. The lines connect points of the predicted O_m-distribution.